ForWind
Zentrum für Windenergieforschung
Bremen
Hannover
Oldenburg

Leibniz
Universität
Hannover

# Probabilistic Safety Assessment of Offshore Wind Turbines

## Annual Report 2012

7th February 2013

Cover: Windturbines on the ocean © Zentilia

| | |
|---|---|
| Research Project: | Probabilistic Safety Assessment<br>of Offshore Wind Turbines (PSA)<br><br>Probabilistische Sicherheitsbewertung<br>von Offshore-Windenergieanlagen (PSB) |
| Sponsored by: | Ministry for Science and Culture in Lower Saxony<br>Niedersächsisches Ministerium für Wissenschaft und Kultur |
| Support Code: | GZZM2547 |
| Research Period: | 01.12.2009 – 30.11.2014 |
| Reference Period: | 01.12.2011 – 30.11.2012 |
| Homepage: | www.psb.uni-hannover.de |

All institutes are members of ForWind and belong to the Leibniz Universität Hannover:

Institute of Concrete Construction
*Prof. Dr.-Ing. Steffen Marx / Dr.-Ing. Michael Hansen (Coordination)*

Institute of Building Materials Science
*Prof. Dr.-Ing. Ludger Lohaus*

Franzius Institute of Hydraulics, Waterways and Coastal Engineering
*Prof. Dr.-Ing. habil. Torsten Schlurmann*

Institute for Geotechnical Engineering
*Prof. Dr.-Ing. Martin Achmus*

Institute for Steel Construction
*Prof. Dr.-Ing. Peter Schaumann*

Institute of Structural Analysis
*Prof. Dr.-Ing. habil. Raimund Rolfes*

Institute for Drive Systems and Power Electronics
*Prof. Dr.-Ing. Axel Mertens / Prof. Dr.-Ing. Bernd Ponick*

Institute of Electric Power Systems
*Prof. Dr.-Ing. habil. Lutz Hofmann*

Institute for Machine Design and Tribology
*Prof. Dr.-Ing. Gerhard Poll*

Insitute of Turbomachinery and Fluid Dynamics
*Prof. Dr.-Ing. Jörg Seume*

# Content

1 Introduction ..... 1

2 Work Packages (WP) ..... 2

2.1 Safety of Offshore Wind Turbines (WP 1) ..... 2

2.2 Action Effects of Wind and Waves (WP 2) ..... 5

2.3 Soil (WP 3) ..... 13

2.4 Foundation and Support Structure (WP 4) ..... 19

2.5 In-Situ Assembly (WP 5) ..... 27

2.6 Monitoring of Mechanical Components (WP 6) ..... 35

2.7 Diagnostic Systems for Electronic Systems (WP 7) ..... 42

2.8 Reliability of the Grid Connection (WP 8) ..... 46

3 Summary ..... 53

4 Literature ..... 54

4.1 Publication List ..... 54

4.2 Doctoral, Diploma, Master and Bachelor Theses ..... 54

# 1 Introduction

**Institute of Concrete Construction**
Michael Hansen, Boso Schmidt

The ForWind research project Probabilistic Safety Assessment of Offshore Wind Turbines is sponsored by the Ministry for Science and Culture in Lower Saxony since 1.12.2009. In this research project safety assessments of the support structure and specific electrical and mechanical components of Offshore Wind Turbines (OWT) are performed. The Annual Report 2010 contains first project descriptions. Annual Report 2011 continues with first results of accomplished work. In this Annual Report 2012 further investigations and outcomes are documented. Safety assessment of OWT is done in several work packages (WP), which are summarized briefly below.

WP 1 provides the frame of this project. Some tools for probabilistic analysis were described in last year annual report. Thus, presently in chapter 2.1 actual developments in code calibration are described.
In WP 2 on the one hand the failure probability of rotor blades of OWTs due to fatigue and ultimate loading is investigated. On the other hand the wave-breaking probability is examined by means of laboratory experiments in two- and three-dimensions to quantify the scatter of the influence factors.
Typical soil conditions, ranges of pile properties and uncertainties are chosen in WP 3 to establish a general approach for modeling axial pile resistance as a single random variable.
WP 4 deals with the foundation and support structure of OWT's. A monopile structure and a jacket structure are implemented and reliability analyses are done for predefined limit state functions. Extreme events are investigated and statistical values of action effects as well as transfer functions for the structural behaviour are determined.
By using methods like Preliminary Hazard Analysis and Fault Tree Analysis the risk factors of the grouted joints during the application process are searched for in WP 5.
In WP 6 the mechanism of bearing damages are achieved by early detection of fatigue in rolling element bearings. Therefore, novel acceleration sensors and analysis procedures are used.
While there are done experimental investigations in WP 6 analogical works are done in WP 7 by simulation. In WP 7 is determined, in how far the detection of faults in electrical machines will be influenced by static or dynamic eccentricities.
In the first part of WP 8 probabilistic models giving information about the failure performance of the offshore grid have been built. The second part contains an approach of resonance analysis including network reduction method.

All project partners are united by methods and input data. Two workshops, with the active participation of representatives of business and certification, took place in Hanover in May and June 2012 to validate the assumptions and previous work in the WPs. On these events the target reliability and critical limit states as well as developments in certification and industry were discussed, too. The results and findings from these discussions are taken into account in the individual work packages.

# 2 Work Packages (WP)

## 2.1 Safety of Offshore Wind Turbines (WP 1)

**Institute of Concrete Construction**
Michael Hansen, Boso Schmidt

### 2.1.1 Motivation

In the field of wind energy and particularly for Offshore Wind Turbines (OWT), there is no international consensus regarding the target reliability. Such reliability index is used for the design of structural components and the total structure, cf. previous annual reports [1], [2]. Expressions concerning the reliability of the structure are included in IEC 61400-1 [3] and EC0 [4] and are nearing to be revised. In addition, especially for offshore structures, the reliability is critically dependent on the availability and accessibility depicted in figure 1.

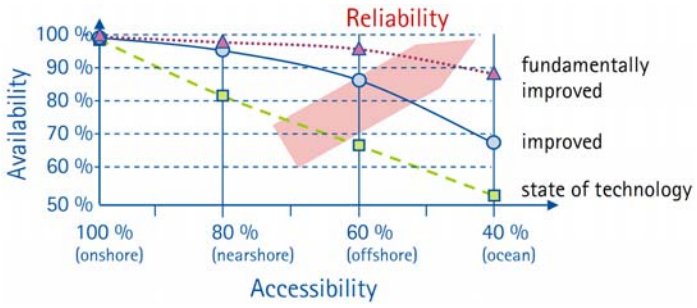


*Figure 1: Dependence between reliability, availability and accessibility for offshore wind turbines, cf. [5]*

The methodology used in the WP as well as the networking between the WP is shown in this Annual Report 2012. Reference is also made to the latest developments regarding the safety approaches.

### 2.1.2 Approach

In WP 2 to 4 usual stochastic models are used as described in previous annual reports [1], [2]. Primarily, simulations are deployed with analysis methods like FORM and Monte Carlo. There are also the response surface method (ARSM) and correlated random fields used in some parts. Details about these methods and applications are contained in the respective WP related publications and presentations. In WP 5 to WP 7, failures in the mechanical or electrical parts or due to construction are monitored. In WP 6, mechanical defects are detected early by measurement. Greater damage to the bearing shall be avoided in this way. The error detection of electrical machines in simulations in WP 7 is similar to that. Winding faults or rotor eccentricities are detected by changes of the electro-magnetic air-gap field. Another field of monitoring is the supervision of the erection. Especially the structural design of joints between the pile and support construction of the OWT is investigated in WP 5. WP 8 deals with consequences of an electrical breakdown in an offshore wind park.

Especially in WP 4 several partners work together to solve interactions of the structure. Validated assumptions for effects, dynamic structural behaviour were done and material parameters of soil and structure were collected. Using these information, realistic limit state functions were analysed.

The probabilistic analysis of limit states and, if applicable, the parallel monitoring of the structural condition, are part of several ongoing investigations [8], [9] and regulations [10]. Particularly, in this context, the target probability of failure leads to an ongoing discussion. In addition to this, the differences between onshore / offshore and the relevant failure mode (brittle / ductile) are of general interest. In committee [10], [11] a target annual probability of failure equal to $P_f = 5 \cdot 10^{-4}$ ($\beta = 3.3$) was considered appropriate.

An informative annex in IEC 61400-1 [3] is planned, which deals with so called "design assisted by testing" [12]. For other structures like buildings or bridges analogous descriptions are included in EN 1990 [4]. For these structures, safety elements were found and calibrated by experimental evaluation. Of course, scale effects are not negligible and have to be taken into account.

### 2.1.3 State of work

There is still no predefined target reliability for wind turbines onshore and offshore. A panel of experts for the BSH standard "design", work group "safety level", met in Hanover in March 2012 [11]. The participants work either for manufacturers, research institutions or certifiers. They met to discuss current and future approaches to safety elements of wind loaded structures and their foundations. As a result, it was indicated that only a risk analysis for the question of optimal safety and reliability of offshore wind turbines may be of primary importance. Within this risk analysis, existing failure probabilities have to be merged together with their (economic) consequences of failure. A target reliability index $\beta$ = 3.3 ($P_{f,annual}$ = $5 \cdot 10^{-4}$) was proposed. But standardized sensitivity factors $\alpha_E$ = –0.7 and $\alpha_R$ = 0.8 set in EC 0 [4] can't be valid any longer because of the dominant wind load. It became apparent, that there is no reasonable basis to reduce the present safety level and associated safety elements of OWT. Thus, holistic investigations for OWT like done in this project are necessary for further approaches.

Supplementary to the works in WP, two workshops, [6] and [7], were held in Hanover in May and June 2012. The aim of these events was to discuss the current approaches and assumptions with representatives from industry and to get to know their interests. Thus, the main focus was set on realistic approaches to the incoming variables in all WP. The question of critical limit states and possible scenarios was discussed once again. The financial losses and the inclusion of public interest were discussed, too. It became clear, that the failure of a single OWT appears to be rather subordinate. However, the failure of a whole wind park seems to be crucial. On the one hand, this refers to the structural design. This occurs e. g. if the towers or the foundation of all OWTs are harmed by a catastrophic event or an inherent systematic failure in design. On the other hand, the failure of the electrical components and the grid connection may lead to big financial losses. Usually, electrical systems used to be planned with a known (N–1)-reliability. This means that each part is designed redundantly. At OWT however, there is no (N–1)-reliability. For these electrical systems, it is not common to keep reserve components for all parts like cables, transformers etc. This is very critical, because for offshore-constructions, the failure of low-cost modules can lead to very high costs of maintenance and repair.

In conclusion, the workshops clarify the interests of industry and enable the validation of assumptions and input values in the current investigations.

Hereinafter, the methods of the different WP shall be brought together step by step. Although there are great differences between used methods in each WP, similarities are recognized.

**References**

[1] PSB-OWEA – Annual Report 2011. Hannover, 2012.

[2] PSB-OWEA – Annual Report 2010. Hannover, 2011.

[3] DIN 61400-1:2005: Windenergieanlagen – Teil 1: Auslegungsanforderungen (IEC 61400-1:2005), Deutsche Fassung EN 61400-1:2005.

[4] EC 0, DIN EN 1990: Grundlagen der Tragwerksplanung; Deutsche Fassung EN 1990:2002 + A1:2005 + A1:2005/AC:2010. Dezember 2010.

[5] Reuter, A.: Impulsvortrag zum Workshop PSB-OWEA „Konstruktion“ am 31.5.2012.

[6] PSB-OWEA – Workshop „Konstruktion“ am 31.5.2012 an der LUH, Hannover.

[7] PSB-OWEA – Workshop „Antriebstrang“ am 14.6.2012 an der LUH, Hannover.

[8] Thöns, S.: Monitoring based condition assessment of offshore wind turbine support structures. Thesis, ETH Zürich, 2011.

[9] Gomez de las Heras, E.; Gutierrez, R.; Azagra, E.; Sorensen, J. A.: Assessment of wind turbines for site-specific conditions using probabilistic methods. EWEA Event 2013, 5.2.2013.

[10] Safety factors – IEC 61400-1 – MT01 Background document, Draft, 16.12.2012.

[11] BSH Standard „Konstruktion“, AG „Sicherheitsniveau“, Protokoll der Besprechung am 20.3.2012 in Hannover.

[12] Sørensen, J. D.: MT1 – SC 'Safety factors': Proposal for informative annex on 'Design assisted by testing'. Roskilde, 22.10.2012.

## 2.2 Action Effects of Wind and Waves (WP 2)

**Institute of Turbomachinery and Fluid Dynamics (TFD)**
Benedikt Ernst, Joerg Seume

**Franzius-Institute for Hydraulic, Waterways and Coastal Engineering (FI)**
Mayumi Wilms, Arndt Hildebrandt, Torsten Schlurmann

For offshore wind turbines (OWTs), aerodynamic wind loads and hydrodynamic wave loads are essential input parameters of probabilistic investigations. Therefore, in this work package characteristic parameters of the loads and the resistance of OWTs will be determined. As a common database, the wind and wave measurements at FINO 1 are used.

### 2.2.1 Motivation (TFD)

The main contributing factors to unsteady loading of OWTs are wind shear, turbulence, and waves. For the design of several mechanical components of OWTs, it is necessary to consider these unsteady loadings and further aeroelastic effects on the entire structure. Examples for these effects are the coupling between the main shaft torsion and the edgewise bending of the blades and the interaction between the tower and the rotor flapwise bending.

### 2.2.2 Approach (TFD)

In this part of the work package, the failure probability of rotor blades of OWTs due to fatigue and ultimate loading will be investigated. In order to do so, 3D turbulent stochastic wind fields are generated based on the FINO 1 data. The aim is to investigate the impact of the wind field parameters on the aeroelastic behaviour of OWTs and on the probability of failure. Furthermore, the sensitivity of the loads and the eigenfrequencies due to variations of structural and/or geometric properties will be investigated.

For the investigations, the aeroelastic model of a 5 MW OWT [1], which was developed at the National Renewable Energy Laboratory (NREL), is used. The wind fields are generated by the simulation software TurbSim [2] and the turbine response is computed with the aeroelastic simulation software FAST [3].

### 2.2.3 State of Work (TFD)

**Site-specific wind field parameters**

In order to investigate the effect of site-specific wind field parameters on the loads of OWTs, the wind speed measurements of the FINO 1 offshore research platform are analysed for the period between January 2004 and December 2010. In [4], 10 min mean wind data of the cup anemometers and the wind vanes are used to derive the turbulence intensity and the wind shear exponent for aeroelastic simulations.

The turbulence intensity $TI$ is defined as the standard deviation $\sigma_v$ of the horizontal wind speed related to the mean wind speed $v$:

$$TI = \frac{\sigma_v}{v}. \qquad (1)$$

At the FINO 1 platform the turbulence intensity is determined by means of the measured standard deviation and the mean wind speed of the cup anemometer at 90 m height. In the IEC standards 61400-1 and 61400-3 [5, 6] the 90th percentile turbulence intensity depending on wind speed is required as an input parameter for the aeroelastic load simulations. Therefore, the FINO 1 data is subdivided into 1 m/s wind speed bins for which the 90th percentiles are calculated. In Figure 1 the measured 90th percentile turbulence intensity is compared with the proposed turbulence intensity in the IEC standard 61400-3 [6]. IEC C onshore denotes the normal turbulence model which can be used for the design of the rotor and nacelle assembly, while IEC C offshore denotes the turbulence conditions

for the design of the support structure. For both relations, a reference turbulence intensity $TI_{15} = 0.12$ is used in accordance with the IEC standard.

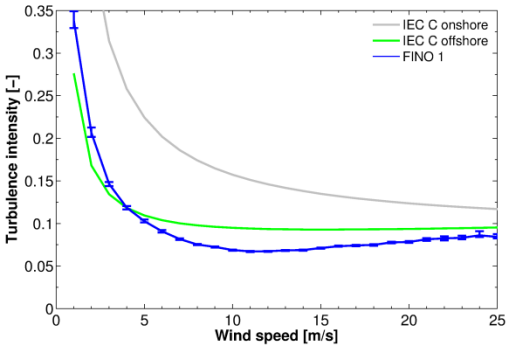


*Figure 1: 90% percentile of the measured turbulence intensity depending on wind speed at 90 m height [4]*

In the IEC standards [5, 6], the wind profile can be described by the so called power law profile:

$$v(z) = v_{hub}\left(\frac{z}{z_{hub}}\right)^{\alpha} \qquad (2)$$

with the mean horizontal wind speed $v(z)$ at the height $z$ above the ground, the mean horizontal wind speed $v_{hub}$ at hub height $z_{hub}$, and the wind shear exponent $\alpha$. The calculation of the wind shear exponent at the FINO 1 platform by means of rearranging Equation 2 is done in two different ways. First, only the mean horizontal wind speeds on two different heights are considered. These are the hub height of the OWT model ($z_{hub} = 90m$) and a height near the lower end of the rotor plane ($z = 40m$). Second, a nonlinear regression over all cup anemometers from 33 m to 100 m height is performed. The hub height of the OWT model is the reference height and for the regression a Levenberg-Marquardt algorithm is used, this leads to more robust wind speed exponents. A comparison of the mean values of the measured wind shear exponents and the recommended value ($\alpha = 0.14$) in the IEC standard [6] are shown in Figure 2.

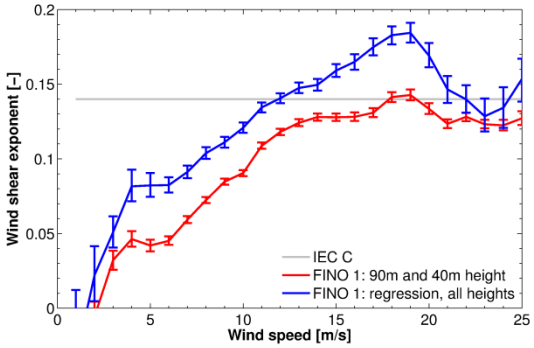


*Figure 2: Mean value of the measured wind shear exponent depending on wind speed [4]*

Using a Kaimal turbulence spectrum, wind fields are generated based on the comparison of the wind field parameters. For each input configuration (mean wind speed, turbulence intensity, wind shear exponent), 30 simulations are performed with 10 min duration and different random seeds. These wind fields are used for aeroelastic load simulations of the 5 MW OWT model.

**Fatigue loads**

The fatigue loads are analysed by means of the damage-equivalent load-range approach. For the time series, rainflow counting is used to determine the amplitudes $R_i$ and the corresponding number of load cycles $n_i$. Based on the IEC standard 61400-13 [7], the damage-equivalent load is defined as

$$\mathrm{R_{eq}} = \left(\frac{\sum_i \mathrm{R_i^{\,m}} \cdot \mathrm{n_i}}{\mathrm{n_{eq}}}\right)^{1/\mathrm{m}} \qquad (3)$$

where $m$ is the Wöhler curve exponent and $n_{eq}$ is the equivalent number of load cycles. The damage-equivalent flapwise and edgewise bending moments at the blade root are calculated with $m = 10$ and $n_{eq} = 600$ for each 10 min time series. This results in an equivalent frequency of 1 Hz. The edgewise bending moment is mainly caused by gravity forces and less affected by turbulence intensity and wind shear. In contrast to this, there are significant differences in flapwise bending moment caused by wind fields which are

based on the IEC standard and the FINO 1 data. As an example, the mean values of the damage-equivalent flapwise bending moments of 30 simulations are shown in Figure 3. Furthermore, it is shown that the bending moments are more affected by turbulence intensity than by the wind shear exponent [4].

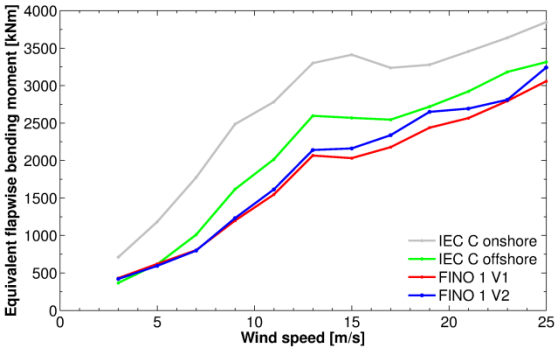


*Figure 3: Mean value of the damage-equivalent flapwise bending moment [4]*

**Extreme loads**

The IEC standards [5, 6] require to determine the extreme loads in an operating state with a recurrence period of 50 years by statistical extrapolation. Ernst and Seume [4] use a Peak Over Threshold extrapolation (POT) method, which is also recommended by the IEC standards [5, 6], and a method based on Average Conditional Exceedance Rates (ACER). In case of the POT method, the threshold is the mean value plus 1.4 times the standard deviation ($\mu + 1.4\sigma$). The aggregation of the peaks is done by means of the "aggregation before fitting" procedure and a three parameter Weibull distribution is used to fit the local distributions. The ACER method is a novel extrapolation method which was developed by Naess and Gaidai [8, 9]. In order to determine extreme loads of wind turbines it was already applied by [10].

For the extrapolation, 30 time series of 10 min duration are available for each input configuration. In order ensure that the extracted peaks are independent, the independency is tested by Blum's test [11] and the sample correlation coefficient.

The characteristic extreme loads obtained by the POT method are generally larger compared with the ACER method. Furthermore, the characteristic of the long-term exceedance distributions differ significantly. Reasons for this are the differences of the POT and ACER method itself as well as the different distribution functions used. In [4] it is shown that the data fits of the POT method are worse compared with fits of the ACER method. Therefore, it is assumed that the characteristic loads obtained by means of the ACER method are more plausible. However, in both cases the simulations based on the IEC standards yield higher characteristic loads compared with simulations based on the FINO 1 data.

**Effect of airfoil geometry variations**

Geometry variations of rotor blades can arise from manufacturing tolerances and operational wear of the blades. In order to investigate the effect of airfoil geometry variations on the lift and drag coefficients as well as the loads and the performance of an OWT, a Latin hypercube sampling is used to vary characteristic parameters simultaneously. These parameters are the maximum thickness, the location of the maximum thickness, the maximum camber, the location of the maximum camber, and the trailing edge thickness. All parameters are normalized with respect to the chord length and varied relatively with respect to the corresponding parameter of the baseline geometry. Except of the variation of the trailing edge thickness, all variations are described by a truncated normal distribution with a mean value of 0% and a standard deviation of 10%. The lower and upper limits are set to +/- 5%, respectively. The trailing edge thickness is very small and therefore also relative changes of +/- 5% would be negligible small. Due to this, a standard deviation of 66,67% is assumed and the lower and upper limits are set to +/- 100%, respectively. For all airfoils of the 5 MW OWT, the lift and drag coefficients are

calculated by means of the panel code XFOIL [12] and the load and performance simulations are performed with FAST [3].
The variations of the airfoil geometry lead to a significant scatter of the lift and drag coefficients (see for example Figure 4) which also affects the damage-equivalent flapwise bending moments. In contrast to that, the effects on the power and the annual energy production are almost negligible with regard to the assumptions made.

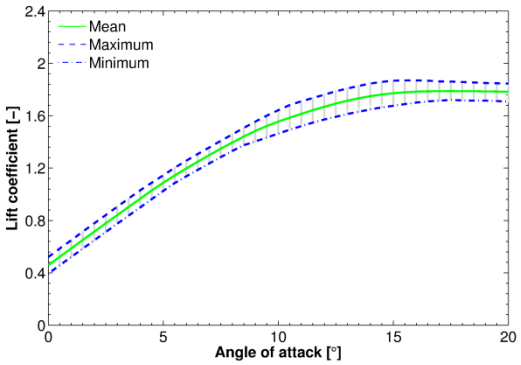


*Figure 4: Lift coefficients of the varied DU25 profile geometries [13]*

**Work in progress**

The rotor blade geometries can vary in many different ways. Therefore, the influence of the radial distribution of the airfoil variances as well as the variation of the chord and twist angle distribution will be investigated. Furthermore, the effect of structural parameters on the aeroelastic behaviour will be analysed.

## 2.2.4 Motivation (FI)

Extreme hydrodynamic loads on OWTs result from breaking waves, which cause severe impact on offshore structures and induce significant singular stresses as well as vibration and therefore discrete degradation of the support structure. The relevant loads for a design base depend on the prevalent sea state (wave height) and geometry characteristics of breaking waves (intensity of impact) in a storm. All influencing factors vary significantly in the natural sea state. For an efficient design of OWTs, dominant and significant sea state parameters as well as wave-breaking probabilities must be considered.

## 2.2.5 Approach (FI)

Validations with measured and computed hindcast data records are necessary and investigations on the laboratory scale are indispensable. In the first step design wave heights and occurrence of wave trains in the North Sea have been analyzed on the basis of statistical analysis of extreme events. The second step deals with the wave-breaking probability, which is investigated by means of laboratory experiments in two- and three-dimensions to quantify the scatter of the influencing factors.

## 2.2.6 State of Work (FI)

Due to the challenge of measuring a spatially and temporally resolved three-dimensional wave field, two-dimensional model tests have been conducted to develop and optimize the measurement system. The main question is “How to detect a breaking wave?”. There are various methods to detect and measure wave-breaking: on one hand the experimental methods which require an in-situ measurement (in the field or laborator, with contact or remote-sensing measurements), and on the other hand theoretical methods which require time series of e.g. surface elevation to analyze analytically or statistically.
Two detection methods are used here: a remote-sensing, optical method and an analytical method. In the following both methods are described.

**Optical detection of wave-breaking**

A video-imagery based system is developed to detect automatically whitecaps in videos taken in a laboratory environment. Whitecaps are here defined as a breaking wave. Several aspects need to be considered: starting with the used cameras, their configuration and calibration aspects, illumination and other environmental influences.

There are a few image-processing techniques for detection of whitecap coverage which basically all work on grayscale-images and the application of thresholds. Stramska and Petelski [14] invented a system to detect whitecaps in the north polar waters using grayscale images. Sugihara et al. [15] are also working with a brightness threshold. Lafon et al. [16] uses an intensity threshold.

In this WP video-records are taken with a Canon-EOS550D. These videos have a resolution of 1920x1080 px and the frame speed is 30 f/s. For further investigations a smaller segment is chosen (751x276 px). Matlab R2007b is used for coding under application of the Image and Map Toolbox. After converting the video to grayscale images (Fig. 1), light pixels are detected in a first step using thresholding or texture analyzing, assuming that pixels of whitecaps are brighter than their surrounding areas. This results in a binary image, representing bright pixels white and so defining possible locations of whitecaps in the image. Beside the whitecap-areas also areas with light reflections or other disturbances are detected here (Fig. 2). These areas need to be filtered in further steps. A dilation is run in the next step to connect all pixels in clusters creating connected components (Fig. 3). In another step components which have a small area (e.g. ca. 0.7m$^2$) are deleted assuming they represent light reflection or disturbance pixels (Fig. 4). The resulting components are labeled (Fig. 5) and investigated in respect of various characteristics for additional filtering. These characteristics can be determined individually for various kinds of whitecapping. First tests have been performed using direction, extent and convexity of detected components, leading to a reduced amount of possible breaking waves. These steps are performed for each frame of the video leading to an amount of possible whitecaps for each frame. Assuming that a whitecap lasts longer than a light reflection, all the detected components need to be traced through all frames. This is realized by calculating the intersection between every component in every frame and its successor. If the intersection is larger than 75 %, the components between the frames are assumed as the same and are connected. If the components are connected through at least e.g. 10 frames (one third second), they are considered as one whitecap. As a result (Fig. 6) we now have a chain of waves through all frames, where all the waves conform to the specifications we have made before. These results are represented in a final video containing original imagery and detected whitecaps marked with white borders.

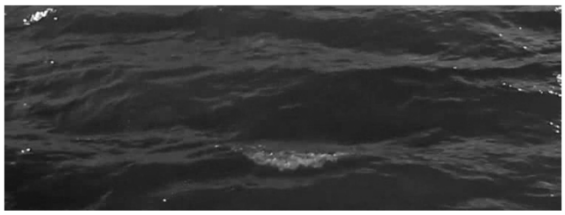

*Figure 1: Videoframe converted to gray*

*Figure 2: Thresholding (creating binary image with white pixels as possible whitecap areas)*

*Figure 3: Dilation (dilate detected pixels to connect pixels to areas)*

*Figure 4: Open area (filter areas of small size)*

*Figure 5: Label (find connected clusters and classify them in respect of aspects like direction, convexity, etc.)*

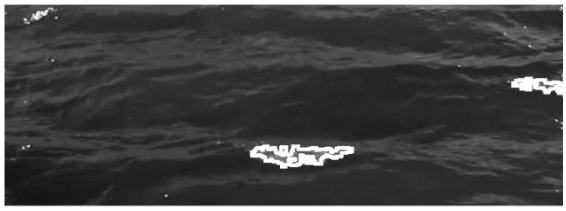

*Figure 6: Final result after filtering for one frame*

**Analytical detection of wave-breaking**

To develop an analytical method, experiments with breaking waves have been caried out in the wave flume (110 x 2.2 x 2 m) of the Franzius-Institute. In the laboratory breaking waves can be generated by focusing waves. This technique is described by Longuet-Higgins [17]. A specific range of wave components is generated and their relative phases adjusted so that the wave energy converge at a spatial location and time, building a large, steep wave which can be forced to break by increasing the steepness of the focused wave.

In the conducted tests six wave gauges are installed to measure the surface elevation. One is fixed at the beginning of the wave flume in a distant of 4.84 m to the wave paddle. The other five wave gauges are installed on a movable wagon ca. 15 m from the wave paddle. The distance between these wave gauges is 0.2 m. The tests are repeated and after every test the wagon is shifted by 0.2 m to get a grid of measured positions and thereby increase the possibility to measure at the location where the wave package focuses or break respectively. To detect wave-breaking in the time series of surface elevation there are theoretical techniques which are semi-empirical due to the complex nature of wave-breaking. Griffin et al. [18] generated breaking waves of varying intensity and used the phase time method, which is based on the Hilbert transform, to determine the location of breaking. They showed that steep waves have a nearly constant Hilbert frequency. When a breaking wave approaches the breaking point, the Hilbert frequency increases. More details to these methods, especially to the Hilbert transform, may be found in Babanin [19] and Huang et al. [20].

In Fig. 7 the Hilbert amplitude (which is the envelope of the surface elevation) is plotted against time for a breaking wave and a non-breaking, focused wave for the location and time of breaking and focusing respectively. For the breaking case the envelope is asymmetric which indicates the breaking.

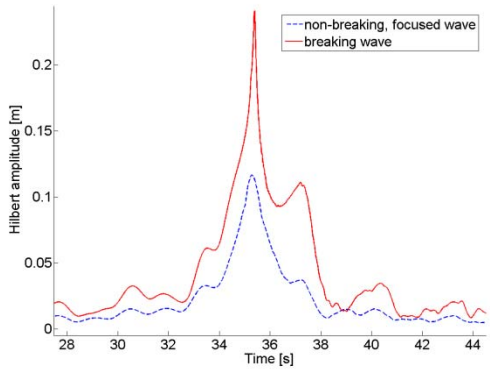


*Figure 7: Hilbert amplitude at the location of focusing and breaking respectively*

In Fig. 8 the Hilbert frequency is plotted against time for a breaking and non-breaking, focused wave for the location and time of breaking and focusing

respectively. For the non-breaking case it may be observed that the Hilbert frequency is nearly constant around the focal point and less than 4 rad/s. For the breaking case the Hilbert frequency increases up to 8 rad/s at the breaking point and decreases afterwards. This corresponds to the results of Griffin et al. [24].

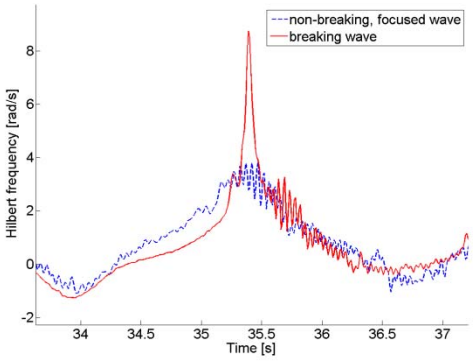


*Figure 8: Hilbert frequency at the location of focusing and breaking respectively*

**Work in progress**

For the further development of the optical detection system several aspects can be considered.

- Optimization of the environmental conditions by e.g. preventing reflections by adjusting the light sources and correcting the position and viewing direction of camera.
- Implementation of a calibration process for the camera.
- Optimization of the code by e.g. extending the filter criteria, reducing the number of used frames.
- By using a second camera, there is the feasibility to create three-dimensional models of the waves. These spatial-information can be used for further filtering of waves and additionally it creates the option to locate the waves in the laboratory and specify the type of breaker (spilling, plunging).

The analytical detection system has to be optimized and more analytical methods have to be tested besides the Hilbert transform.

**References**

[1] Jonkman, J.; Butterfield, S.; Musial, W.; Scott, G.: Definition of a 5-MW Reference Wind Turbine for Offshore System Development. National Renewable Energy Laboratory: NREL/TP-500-38060, 2009.

[2] Jonkman, B.J.: TurbSim User's Guide: Version 1.50. National Renewable Energy Laboratory: NREL/TP-500-46198, 2009.

[3] Jonkman, J.M.; Buhl Jr., M.J.: FAST User's Guide. National Renewable Energy Laboratory: NREL/TP-500-38230, 2005.

[4] Ernst, B; Seume, J.R.: Investigation of Site-Specific Wind Field Parameters and Their Effect on Loads of Offshore Wind Turbines. Energies 2012, 5, 3835-3855, doi: 10.3390/en5103850.

[5] International Electrotechnical Commission: IEC 61400-1: Wind turbines part 1: Design. 3rd edition, 2005.

[6] International Electrotechnical Commission: IEC 61400-3: Wind turbines part 3: Design Requirements for Offshore Wind Turbines. IEC, 1st edition, 2009.

[7] International Electrotechnical Commission: IEC TS 61400-13: Wind Turbine Generator Systems Part 13: Measurement of Mechanical Loads; 1st edition, 2001.

[8] Naess, A.; Gaidai, O.: Monte Carlo Methods for Estimating the Extreme Response of Dynamical Systems. J. Eng. Mech. 2008, 134, 628--636.

[9] Naess, A.; Gaidai, O.: Estimation of extreme values from sampled time series. Struct. Saf. 2009, 31, 325-334.

[10] Toft, H.S.; Naess, A.; Saha, N.; Sørensen, J.D.: Response Load Extrapolation for Wind Turbines During Operation Based on Average Conditional Exceedance Rates. Wind Energy 2011, 14, doi: 10.1002/we.455.

[11] Blum, J.R.; Kiefer, J.; Rosenblatt, M.: Distribution free tests of independence based on the sample distribution function. Ann. Math. Stat. 1961, 32, 485-498.

[12] Drela, M.; Youngren, H.: XFOIL 6.94 User Guide, Cambridge, MA, USA: Massachusetts Institute of Technology, 2001.

[13] Ernst, B.; Schmitt, H., Seume, J.R.: Effect of Geometric Uncertainties on the Aerodynamic Characteristic of Offshore Wind Turbine Blades. Presentation: The Science of Making Torque from Wind, October 9-12, 2012, Oldenburg, Germany.

[14] Stramska, M. and T. Petelski: Observations of oceanic whitecaps in the north polar waters of the Atlantic. *J. Geophys. Res.*, 108(C3), 3086, 2003.

[15] Sugihara, Y.; Tsumori, H.; Ohga, T.; Yoshioka, H.; Serizawa, S.: Variation of whitecap coverage with wave-field conditions. *Journal of Marine Systems*, 66, 47–60, 2006.

[16] Lafon, C.; Piazzola, J.; Forget; P.; Le Calve, O.; Despiau, S.: Analysis of the Variations of the Whitecap Fraction as Measured in a Coastal Zone. Boundary-Layer Meteorology, 111(2):339-360, April 2004.

[17] Longuet-Higgins, M.: Breaking waves – in deep or shallow water. Proc. 10th Conf. Naval Hydrodynamics, Cambridge, MA, Massachusetts Institute of Technology, 597-605, 1974.

[18] Griffin, O.; Peltzer, D.; Wang, T.: Kinematic and dynamic evolution of deep water breaker waves. Journal of geophysical Research, 101, C7, 16, 515-16, 531, 1996.

[19] Alexander Babanin: Breaking and Dissipation of Ocean Surface Waves. Cambridge University Press, New York, 2011.

[20] Huang, N.E.; Shen, Z.; Long, S.R.; et al.: The empirical mode decomposition and the Hilbert spectrum for nonlinear and non-stationary time series analysis. Proc. R. Soc. Lond. A454, 903-995, 1998.

## 2.3 Soil (WP 3)

**Institute for Geotechnical Engineering**
Martin Achmus, Kirill Schmoor

By performing geotechnical reliability based design one of the major tasks is the establishing of a suitable soil model. This is due to heterogeneity and spatial variation of certain soil properties for a considered area not always a straight forward task.
For geotechnical problems which affect only a relative small region (like footing calculations) the soil properties are often modeled by using one single variable which represents the property for the whole considered soil area. In case of other geotechnical problems (like slope stability or pile foundations) where a larger spatial region has to be taken into account, it is suitable to model the soil as a random field. This would lead to a more complex model and computational effort but in reverse a more reliable response can be expected, since a more detailed soil structure is implemented. This also allows determining local failure mechanisms of a global system.

### 2.3.1 Motivation

One of the aims of this work package is to reduce the effort of modeling a random field soil model for reliability analysis of axially loaded offshore foundation piles in the North Sea soil conditions.
For this a parameter study with a 1-D autocorrelated random field soil model for two different soil densities was performed where the distributions of the axial resistances were evaluated. Further a recommendation for modeling the axial pile resistance as a function of deterministic variables like the embedded pile length and pile diameter is presented.
That means that the distribution of the axial resistance can be modeled according to the proposed recommendations directly as a single random variable without facing the difficulties arising from a more complex soil model. Hence, the proposed results can be seen as an interface for other disciplines and work packages, respectively.

### 2.3.2 Approach

**Introduction**

For water depths from $25 - 30\,m$ mainly Jacket and Tripod structures are planned to be installed in the North Sea, since for greater water depths these types of constructions seems to be more suitable compared to Monopiles.
Due to the shape and a certain footprint of these structures the horizontally acting environmental forces are transferred axially into the foundation piles. Because of that the pile bearing capacity results primarily via shaft friction and in case of compression loading additional from pile tip resistance. For most loading conditions the tension case is the controlling one, since the resistance arises only from shaft friction which is also lower than for compression conditions.
The pile resistance in tension can be obtained from eq. (1). Due to varying stress states of the inner soil in the pile two different boundary conditions are defined by the API to determine the axial resistance. By assuming full plugging of the inner soil the resistance is composed of the outer shaft friction load and the unit weight of the inner soil plug. In the other case the resistance consists of the outer and inner shaft friction load.

$$R_k = \min \begin{cases} \int_0^L f(z) \cdot A_o \, dz + G_{plug} \\ \int_0^L f(z) \cdot (A_o + A_i) \, dz \end{cases} \quad (1)$$

where:

| | |
|---|---|
| $f(z)$ | Shaft friction at depth z |
| $A_o$ | Outer shaft friction area |
| $A_i$ | Inner shaft friction area |
| $G_{plug}$ | Unit weight of the inner soil plug |
| $L$ | Embedded pile length |

| Ralative density description | Ralative density | Shaft friction factor β [-] | Limiting shaft friction values $f_{lim}$ [kN/m²] |
|---|---|---|---|
| Very loose – Loose | 0.00 – 0.35 | Not applicable | Not applicable |
| Medium dense | 0.35 – 0.65 | 0.37 | 81 |
| Dense | 0.65 – 0.85 | 0.46 | 96 |
| Very dense | 0.85 – 1.00 | 0.56 | 115 |

*Table 1: Design parameters for sand*

The shaft friction of offshore foundation piles in sand for tension conditions can be computed by eq. (2) acc. to the guideline of the American Petroleum Institute (API) [1]:

$$f(z) = \min \begin{cases} 2/3 \ \beta \cdot \sigma_v'(z) \\ 2/3 \ f_{lim} \end{cases} \qquad (2)$$

where:

$\beta$ Dimensionless shaft friction factor
$\sigma_v'(z)$ Effective vertical stress at depth z
$f_{lim}(z)$ Limiting shaft friction value

The shaft friction factors as also the limiting shaft friction values depend on the relative density of the sand and may vary with depth. Table 1 summarizes the values recommended by the API. It should be mentioned that the additional factor of $2/3$ is prescribed by certification companies like the Germanischer Lloyd (GL) [4].
To estimate the relative density the proposed approach by Jamiolkowski et al. is recommended by the API. Therefore a CPT investigation has to be performed and evaluated which already is demanded as a required field test by the BSH [2].

$$D_r = \frac{1}{2.93} \ln\left(\frac{q_c}{205 \ \sigma_m(z)^{0.51}}\right) \qquad (3)$$

where:

$q_c$ CPT cone tip resistance in kN/m²
$\sigma_m(z)$ Soil effective mean in-situ stress at depth z in kN/m²
$\sigma_m(z) = \left(\sigma_v'(z) + 2 \ \sigma_h'(z)\right)/3$
$\sigma_h'(z)$ Effective horizontal stress at depth z
$\sigma_h'(z) = \sigma_v'(z) \ K_0$
$K_0 = 1 - \sin\varphi'$

**Assumed Conditions**

For the performed study typical site conditions for the North Sea and typical ranges for the foundation pile properties were assumed.
Since the subsoil in the German North Sea mostly consists of dense sands with only limited intermediate cohesive layers, an idealized homogeneous dense ($D_r = 0.75$) and very dense ($D_r = 0.93$) sand profile were considered.
The choice of pile properties depends on the type of foundation, the water depth and the subsoil condition at the desired location. General it can be said that slenderness ratios between $L/D = 10$ and $L/D = 40$ were used. Thereby the pile diameter is varying between $D = 1 - 3m$ where the pile embedded length is commonly chosen to be between $L = 20 - 60m$. For better identification of possible trends also two data pairs of the pile diameter and length were computed which are beyond the mentioned slenderness ratios (set in parentheses in table 3).
As already mentioned above the controlling limit state in most design conditions is the tension load case, in which the piles are suggested to behave plugged. The presented results also based on that assumption.

**Soil model**

In the first PSB Annual Report 2010 (WP3) already a brief description is given on random field modeling [8]. Hence, an introduction to that topic is not given here. The applied soil model for the performed study mainly bases on a 1-D autocorrelated field for the cone tip resistance. Therefore a constant inherent variability $w(qc)$ for a CPT profile was modeled every $0.5\,m$ where an auto-

correlation length of $\theta = 0.6\,m$ with an exponential autocorrelation function acc. to eq.(4) was chosen for all calculations.

$$\rho = e^{\left(-\frac{\Delta x}{\theta}\right)} \qquad (4)$$

where:

| | |
|---|---|
| $\rho$ | Correlation between all points which are separated by distance $\Delta x$ |
| $\Delta x$ | Distance between points |
| $\theta$ | Autocorrelation length |

Since only a 1-D field was simulated the correlation structure was computed by applying the Cholesky technique acc. to eq.(5) [3]. Herein $L$ represents the lower triangular resulting of the Cholesky decomposition of the correlation matrix. The established autocorrelation structure is shown in figure 1.

$$y = L \cdot x \qquad (5)$$

where:

| | |
|---|---|
| $y$ | Correlated random field |
| $L$ | Lower Cholesky decomposition of the correlation matrix |
| $x$ | Uncorrelated random field |

CPT profiles for a constant density of $D_r = 0.75$ and $D_r = 0.93$ were used as trend functions $t(qc)$. Also a measurement error for the cone tip resistance $e(qc)$ was applied. Figure 2 shows as example one realization of a simulated CPT profile $twe(qc)$ with the assumed trend function for dense soil conditions ($D_r = 0.75$). In addition also the corresponding relative density profiles are elucidated.

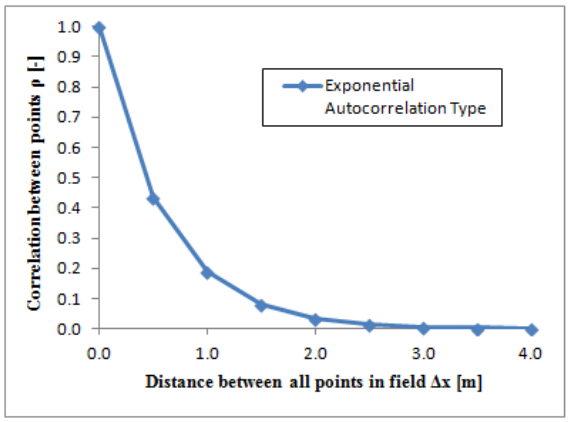


*Figure 1: Autocorrelation structure of random field with $\theta = 0.6\,m$*

**Probabilistic parameters**

For all performed simulations of each data set one million realizations were computed to achieve a convincing response.

The inherent variability of the cone tip resistance $w(qc)$ was assumed to be constant with depth. By applying a standard deviation of $6000 kN/m^2$ the COV is varying between $0.75 - 0.20$ for dense and $0.40 - 0.10$ for very dense soil conditions. According to Phoon et al. [6] the COVs are thereby in a typical range of $0.81 - 0.10$. The vertical autocorrelation length for the cone tip resistance $qc$ is indicated to be between $0.05 - 0.12m$.

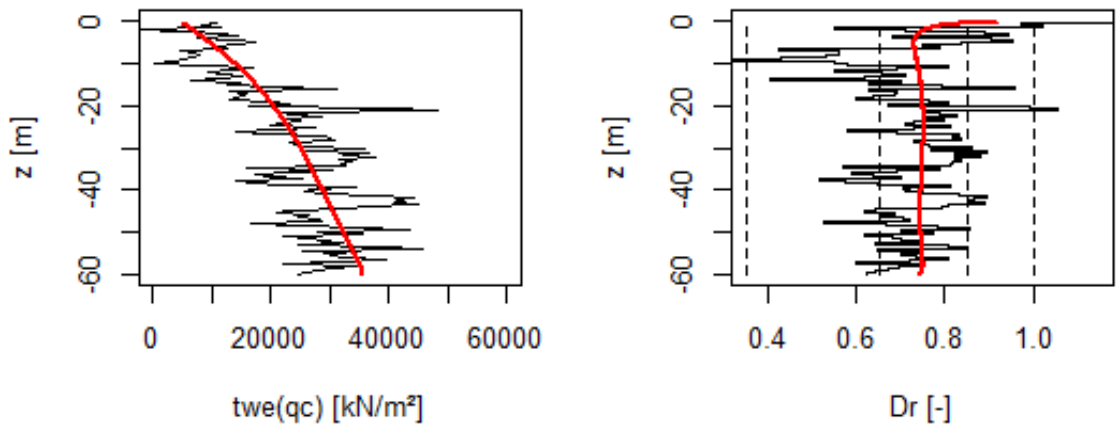


*Figure 2: Simulated CPT profiles with corresponding relative density profiles*

| Basic variable | Notation | Mean | SD | COV | Distribution type |
|---|---|---|---|---|---|
| Unit weight | $\gamma'$ | $10\ kN/m^3$ | $1\ kN/m$ | 0.10 | Normal |
| Inherent variability | $w(qc)$ | - | $6000\ kN/m^3$ | $0.75-0.10$ | Normal |
| Measurement error | $e(qc)$ | 1 | 0.15 | 0.15 | Normal |
| Transformation error $\varphi'$ | $te(\varphi')$ | $0°$ | $2.8°$ | 0.07 | Normal |
| Pile diameter | $D$ | $1-3\ m$ | - | - | Deterministic |
| Pile length | $L$ | $20-60\ m$ | - | - | Deterministic |
| Pile wall thickness | $t$ | $D/40$ | - | - | Deterministic |

*Table 2: Stochastic parameters used for MCS*

Hence, the mean value of $\theta = 0.6m$ was chosen for all simulations.
The unit weight $\gamma'$, the measurement error for the cone tip resistance $e(qc)$ and the transformation error for the internal friction angle $te(\varphi')$ were modelled as uncorrelated and normal distributed random fields with typical values for the mean and standard deviation. All applied variables with their corresponding stochastic moments are summarized in table 2.

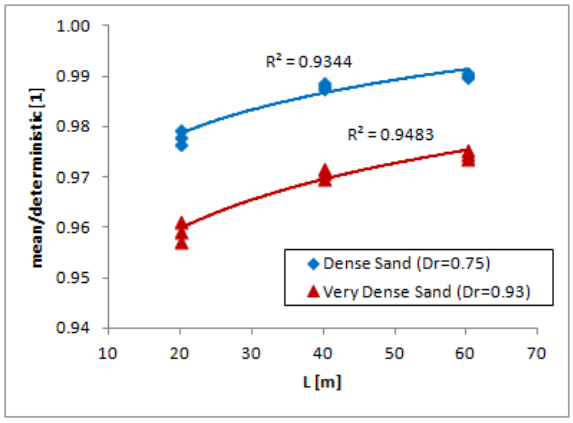


*Figure 3: Related mean value as function of the embedded pile length for all diameters*

## 2.3.3 State of Work

### Mean value

Firstly, table 3 shows the computed pile resistances without considering uncertainties. Hence, only the trend functions of both densities for the cone tip resistance and the mean value of the unit weight were taken into account.
As it can be seen from figure 3 the mean values of the resulting distributions are close to the deterministic computed ones. A small dependency with the embedded pile length can be noticed. General it can be said that the longer the pile is assumed the closer is the mean of the corresponding resistance distribution to the deterministic value.

### Deviation

The variability of the relative density obtained from direct measurements for dense to very dense soil conditions is illustrated in [6] to be between $COV = 0.15 - 0.09$. This shows a good agreement with the computed variation of the relative density from evaluating the simulated CPT simulations. Figure 4 shows a distribution for the COV of the relative density and the corresponding distribution for the resistance. Due to the robust formulation for obtaining the resistance by the API the COV of the resistance is much lower than for the density. Hence, the segment definition for the shaft resistance is less resistant to variations in soil condition.

| $R_{D_r=0.75}/R_{D_r=0.93}$ | $L = 20m$ | $L = 40m$ | $L = 60m$ |
|---|---|---|---|
| $D = 1m$ | $2117\ kN\ /\ 2546\ kN$ | $6279\ kN\ /\ 7505\ kN$ | $(10442\ kN\ /\ 12464\ kN)$ |
| $D = 2m$ | $4518\ kN\ /\ 5376\ kN$ | $13124\ kN\ /\ 15577\ kN$ | $21733\ kN\ /\ 25778\ kN$ |
| $D = 3m$ | $(7202\ kN\ /\ 8489\ kN)$ | $20537\ kN\ /\ 21216\ kN$ | $33876\ kN\ /\ 39943\ kN$ |

*Table 3: Deterministic pile resistances for dense and very dense soil conditions as functions of the pile length and pile diameter*

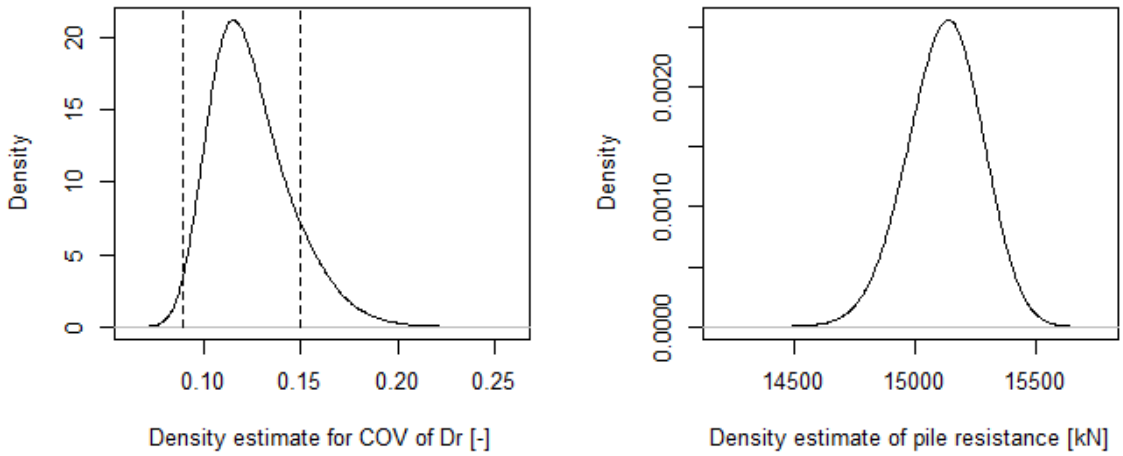


*Figure 4: COV distribution of the relative density with corresponding distribution of the resistance for very dense sand with $L = 40m$ and $D = 2m$*

Nevertheless the COVs for the pile resistances show a correlation to the embedded pile length as can be seen from figure 5. With increasing pile length the variation in the resistance is decreasing.

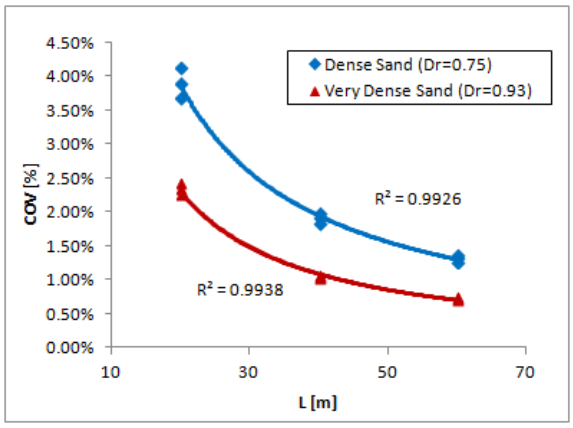


*Figure 5: COV of the resistance as function of the embedded pile length for all diameters*

**Distribution type**

By evaluating Q-Q plots it could be determined that for all cases with dense soil conditions a Gaussian distribution for the pile resistance can be assumed. For very dense soil conditions it could be recognized that the resistance more probably does not follow a normal distribution. Figure 6 shows a standard normal Q-Q plot for both soil densities.
However, a normal distributed resistance also for very dense sand seems to be the best estimate distribution type. Further researches are needed to make a more accurate statement.

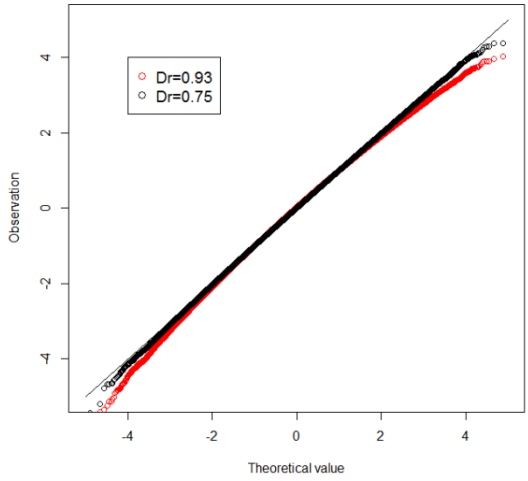


*Figure 6: Standard normal Q-Q plot of the pile resistances with $L = 40m$ and $D = 2m$*

**Does autocorrelation matter?**

To investigate if an autocorrelation structure has any effects on the results two additional calculations without uncorrelated random fields for both density conditions were performed.
General it can be said that in both cases the mean value was the same. The autocorrelation had only an effect on the standard deviation and the shape of the resulting distribution. Without an auto-correlation the deviation decreases and the skewness of the shape tends to zero, as it would be expected. Figure 7 shows both density functions in comparison.

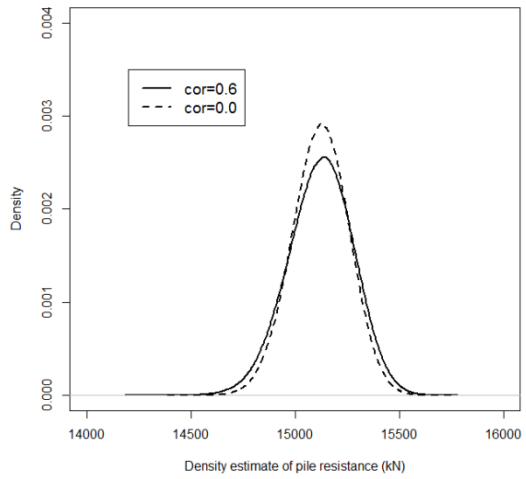


*Figure 7: Density of pile resistance for very dense sand with $L = 40m$ and $D = 2m$*

**Conclusion**

Typical soil conditions, ranges of pile properties and uncertainties were chosen to establish a general approach for modeling axial pile resistance as a single random variable.

Therefore the following steps are recommended to simulate the pile resistance distribution:

1) Choose pile length and diameter
2) Calculate deterministic pile resistance
3) Interpolate mean value from Fig. 3
4) Interpolate COV value from Fig. 5
5) Model resistance distribution with the obtained values as normal distributed variable

It should be noticed that the so computed distribution is based on the above mentioned assumptions and limitations. Therefore it is not recommended to transfer general conclusions to other soil or pile systems.

**References**

[1] API: ecommended Practice for Planning, Designing and Constructing Fixed Offshore Platforms- Working Stress Design, API (RP2A-WSD); Dallas: American Petroleum Institut, 21st edition, 2006

[2] Bundesamt für Seeschifffahrt und Hydrographie (BSH) - Standard Baugrunderkundung für Offshore-Windenergieparks, April 2008

[3] Fenton, G. A.; Griffiths, D. V.: Risk Assessment in Geotechnical Engineering, John Wiley & Sons, 2008

[4] Germanischer Lloyd (GL-COWT), Rules and Guidelines IV - Industrial Services, Part 2 Guideline for the Certification of Offshore Wind Turbines, Edition 2010.

[5] Phoon, K.-K.: Reliability-based design in geotechnical engineering; Abingdon, New York: Taylor & Francis, 2008

[6] Phoon, K. K.; Kulhawy, F. H.: Characterization of geotechnical variability, Canadian Geotechnical Journal, 36, pp. 612-624, 1999a

[7] Phoon, K. K.; Kulhawy, F. H.: Evaluation of geotechnical property variability, Canadian Geotechnical Journal, 36, pp. 625-639, 1999b

[8] Probabilistic Safety Assessment of Offshore Wind Turbines, annual report 2010, Leibniz Universität Hannover, February 2011.

## 2.4 Foundation and Support Structure (WP 4)

**Institute for Steel Construction**
Peter Schaumann, Sebastian Kelma

**Institute of Structural Analysis**
Raimund Rolfes, Jan Goretzka

**Institute of Concrete Construction**
Boso Schmidt, Michael Hansen

### 2.4.1 Motivation

Work Package 4 (WP 4) deals with design and optimization of support structures of offshore wind turbines (OWTs) with respect to probabilistic methods.
Loads acting on the turbine are transferred by the support structures of OWTs into the soil. Besides dead loads of the rotor nacelle assembly (RNA) and support structure, operation loads of the RNA as well as wind and wave induced loads have to be transferred to the soil.
The design of support structures shows small scatter with regards to material and geometry, as already stated in [1]. In contrast, loads from wind and waves as well as the load bearing capacity of the soil are afflicted with great uncertainties.
These uncertainties within design and optimization of support structures are considered by applying probabilistic methods and shall be investigated within WP 4.

### 2.4.2 Approach

Besides monopiles, more complex substructures such as jackets have been investigated. The maximum pile resistance for tension loading is one design-driving limit state. The objective was to find the ultimate limit state function for the pile resistance for tension loading in cooperation with WP3 (soil).
In a first step, an idling OWT during an one-year storm is analysed. The environmental conditions of an one-year storm as well as their statistical properties are already compiled on basis of the environmental data from the FINO1 measuring platform (cf. [2]).
Scattering parameters to describe the wind (mean wind speed, turbulence intensity, etc.) and the sea state (significant wave height, wave period, etc.) are considered in numerical simulations which are carried out to calculate the extreme response of an OWT.
For numerical simulations, wind and wave induced loads acting on the OWT are determined separately and independently of each other, as it is proposed in [3]. The fully-coupled simulation of the OWT, which can be carried out by the coupling of Poseidon and Flex5 [4], is too time-consuming due to scattering input parameters. Nevertheless, the conditions of this approach still must be validated.
In order to find the distribution of the extreme load acting on a pile, wind and wave induced loads depending on the environmental parameters are taken into account. This distribution shall be compared to the maximum pile resistance for tension loading in accordance to [5], which depends on the pile and soil properties.
Robustness and modal analysis of a monopile with varying soil properties was finalized and has been presented at the 8th PhD Seminar on Wind Energy in Europe [6].

### 2.4.3 State of Work

**Modelling**

Data for a wind turbine are taken from the NREL 5-MW Turbine definition [7], which was used within the OC3 project [8]. The hub height above mean sea level (MSL) is 90.55 m.
The chosen jacket substructure was used within the OC4 project [9], as seen in figure 1. This jacket is designed for a site at the North Sea with a local water depth of 50 m. It is connected to the seabed by foundation piles, whose dimensions are given in [9]. The piles are not modelled for the numerical investigations, but the model of the jacket is hinged at the seabed. Using this approach the tension and compression forces acting on the

foundation piles, which are the point of interest, are slightly overestimated.
The transition piece of the OC4 jacket is a concrete block as can be seen in figure 1. The transition piece is modelled as an assembly of beams and masses which represents the structural properties of the concrete transition piece.

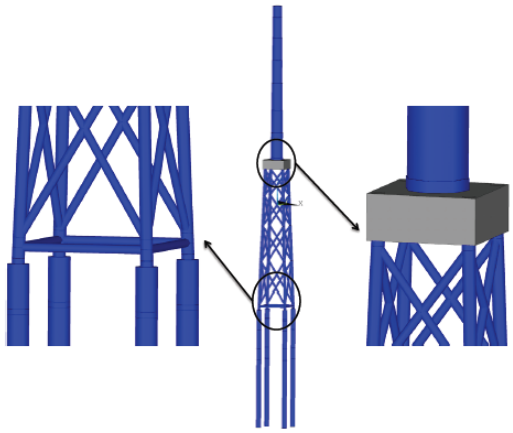

*Figure 1: OC4 jacket (middle), foundation piles (left) and transition piece (right) [9]*

The loading direction is assumed to act over the diagonal of the jacket, which creates the largest pile loads. In order to determine wave loads acting on the jacket, the structure of OWT, including tower and RNA, is modelled by applying the FE code Poseidon [4]. The wind induced loads acting on the RNA and the tower are calculated by using the program Flex5.

**Loading**

In order to find the statistical properties of the wind induced loads, one-hour time series were generated using Flex5-Poseidon coupling and were evaluated considering the extreme wind loads acting on the piles.
For wind speeds at hub height, which possibly occur during an one-year storm, fully-dynamic simulations are carried out to find the mean value and the standard deviation of the wind induced loads, which are almost constant for a constant mean wind speed. Based on the FINO1 data, a Gumbel distribution of the extreme wind speed is assumed (cf. [2], grey line in figure 2),

$$F_u(x) = exp\{-exp[-a \cdot (x-u)]\}, \quad (1)$$

with parameters $u$ and $a$ for a one-year-storm. Further evaluation of the FINO1 data also indicates that the turbulence intensity $TI$ as well as the wind-shear factor $\alpha$ are almost constant for high wind speeds. Hence, these values are set to $TI = 10\%$ and $\alpha = 0.14$, respectively.
Figure 2 shows the mean value and standard deviation for each wind speed investigated.

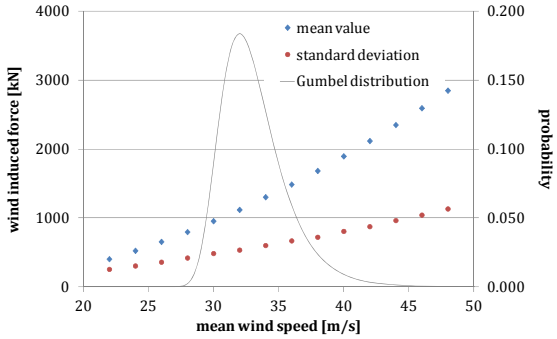


*Figure 2: Mean value and standard deviation of the wind induced tension force acting on the pile depending on the mean wind speed at hub height*

Besides the mean value, the standard deviation increases with increasing wind speed. The same observation is made for the extreme value (not shown in figure 2). The parent distributions of the extreme wind induced loads are weighted by the distribution of the wind speed occurring during an one-year storm.
In order find the parent distribution of the extreme wind induced loads, two different stochastic methods are applied (cf. [10]). The extreme value theory, which was used in [3], is very time consuming, since many time series have to be generated and evaluated. A Gumbel distribution was applied to describe the stochastic behaviour of the extreme wind induced loads. Considerably less time series are necessary for the peak-over-threshold method, but unfortunately some problems occur, which still must be solved to justify the application of this method.

Wave induced loads depend on various parameters. Therefore, some assumptions have been made for the simulations. Results for wave induced pile tension are only valid for the considered jacket in a water depth of 50 m and a significant wave height up to 12 m. This is sufficient for the considered location in the North Sea. First, static analyses are carried out. Doing this, increasing loads due to dynamic system response are not considered. Due to the stiffness of the jacket and its transparency to waves this approach is acceptable, cf. [3]. The connection between significant wave height $H_S$ and maximum wave height $H_{max}$ is assumed to eq. (2) according to valid regulations [11], [12], [13].

$$H_{max} = 1.86 \cdot H_s \tag{2}$$

The wave period $T$ has to be set reasonably because it affects the wave load. The GL [11] and other regulations [12], [13] propose a period range depending on significant wave height according to eq. (3).

$$11.1\sqrt{H_s/g} \leq T \leq 14.3\sqrt{H_s/g} \tag{3}$$

In case of static analysis the minimum wave period generates maximum axial pile loads. Using the lower bound of eq. (3), eq. (4) can be found for maximum pile loads depending on significant wave height, cf. figure 3.

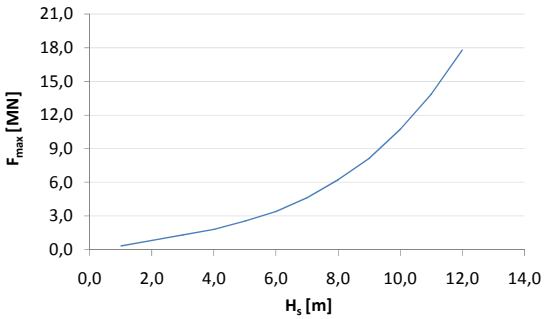


*Figure 3: Maximum pile tension of the OC4 jacket depending on different significant wave heights $H_s$*

$$F_{max} = 0.013 \cdot H_s^3 - 0.095 \cdot H_s^2 + 0.711 \cdot H_s - 0.317 \tag{4}$$

The simulations were performed with a Dean/Dalrymple stream function 11th order [14], whereby all wave heights and periods are covered, cf. [12, Figure C.1].
By using eq. (4), the distribution of effecting pile tension depending on significant wave height can be determined and compared with the associated resistance of the soil. The distribution of significant wave height at the site of FINO1 has already been investigated and can be found in Table 1.

*Table 1: Statistical values (mean $m_{Ext}$ and standard deviation $\sigma_{Ext}$) of the one-year extreme value distribution of $H_S$ at the site of FINO1*

| parameter | distribution | $m_{Ext}$ [m] | $\sigma_{Ext}$ [m] |
|---|---|---|---|
| $H_S$ | Gumbel | 7.091 | 1.311 |

The environmental data from the FINO1 platform are only valid for this site with a local water depth of 28 m. They have to be adapted to a water depth of 50 m for the intended probabilistic calculations at OC4 jacket.

The Shore Protection Manual [15] offers an opportunity to adapt the significant wave height. Mentioned there equations are used to predict sea conditions depending on wind speed, fetch length and wind duration. So called fetch diagrams illustrate these parameters for deep- and shallow water. Both areas are distinguished by the ratio of water depth $d$ and wavelength $L$.

$$\text{Deep water: } \frac{d}{L} \geq 0.5 \tag{5}$$

$$\text{Shallow water: } \frac{d}{L} < 0.5 \tag{6}$$

Shallow water is considered for a water depth of 50 m already at a wavelength of 100 m. Because the adaption is being done in the context of extreme value considerations with wave length of more than 200 m, the prediction method for shallow water will be considered, cf. eq. (7) – (9).

$$\frac{g \cdot H_{m0}}{U_A^2} = 0.283 \cdot tanh\left[0.530 \cdot \left(\frac{g \cdot d}{U_A^2}\right)^{3/4}\right] \cdot tanh\left\{\frac{0.00565 \cdot \left(\frac{g \cdot F}{U_A^2}\right)}{tanh\left[0.530 \cdot \left(\frac{g \cdot d}{U_A^2}\right)\right]}\right\} \quad (7)$$

$$\frac{g \cdot T_p}{U_A} = 7.540 \cdot tanh\left[0.833 \cdot \left(\frac{g \cdot d}{U_A^2}\right)^{3/8}\right] \cdot tanh\left\{\frac{0.0379 \cdot \left(\frac{g \cdot F}{U_A^2}\right)^{1/3}}{tanh\left[0.833 \cdot \left(\frac{g \cdot d}{U_A^2}\right)^{3/8}\right]}\right\} \quad (8)$$

$$\frac{g \cdot t}{U_A} = 5.370 \cdot 10^2 \cdot \left(\frac{g \cdot T_p}{U_A}\right)^{7/3} \quad (9)$$

with:

$H_{m0}$: corresponds to $H_S$, cf. [15]
$U_A$: mean wind speed in the period $t$ at 10 m height
$F$: fetch length
$T_p$: peak period
$t$: wind duration.

The influence of water depth can be estimated assuming constant wind conditions, i.e. same wind speed and fetch length.
The extreme wind speed $U_A$ of duration $t$ is determined from FINO1 measurement data. The fetch length for the site of FINO1 measurement platform lies between 50 and 850 km [16] depending on wind direction. The variation of significant wave height for the increase of the water depth from 28 to 50 m is illustrated in figure 4.

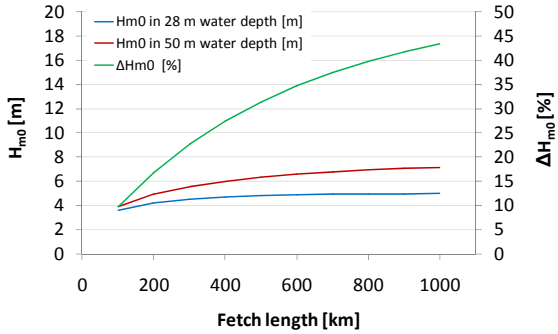


*Figure 4: Wave height $H_{m0}$ and percentage change of $H_{m0}$ for the increase of water depth from 28 to 50 m depending on fetch length*

Using figure 4 the mean value of significant wave height at the site of FINO1 can be adapted to a site with 50 m water depth. An adaption of the standard deviation to the water depth of the OC4 jacket is still pending.

**Robustness Analysis for the structural behaviour of a Monopile**

The first support structure investigated within work package 4 included a monopile substructure (cf. [1], [2]). Robustness analysis was carried out in order to predict the influence of various input parameters (material parameters, geometry of the structure and composition of the soil layer) on the vibration behaviour of the OWT. Within these modal analyses, numerical models with different boundary conditions for soil-pile interactions are implemented (cf. [6]). The numerical model consists of tower with top mass, monopile and foundation (see figure 5). Therein, the design basis was assembled from different published reports [8] [17] and adapted to fulfil the environmental conditions of the German North Sea at the location of FINO1 (cf. [2]).

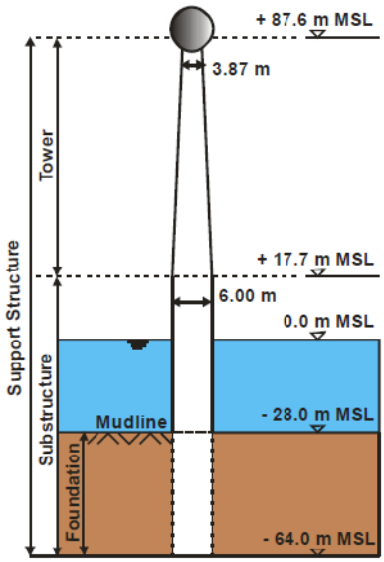


*Figure 5: Investigated support structure of the OWT with monopile substructure*

For the foundation, two different types of bearings are modelled. In a first investigation (model S1), the monopile has a clamped bearing at mudline and no soil-pile interactions are examined. The results of the modal analysis are compared to the investigations in [8]. In a second step a more sophisticated soil model (model S2) is used. Within this implementation, soil-pile interactions are modelled with spring and damper elements. The spring stiffness in dependence of the soil layer is calculated with a program developed at the Institute for Geotechnical Engineering at the Leibniz Universität Hannover using the nonlinear $p$-$y$ theory for sand under cyclic loading conditions as defined by the American Petroleum Institute [5]. The results of the modal analysis with the sophisticated soil model (model S2) are compared to the investigations in [17]. The first and second natural bending frequencies of the support structure (fore-after and side-to-side modes) are shown in table 2.

The specification of the foundations' behaviour at sea is more complex and rather difficult than on land. Reliable data on the soil conditions are hardly to obtain for the offshore sector.

*Table 2: Natural bending frequencies of the support structure (in Hz) of the two analyzed models compared to similar investigations in [17]. Mean values for the soil parameters of model S2 have been assumed (see Table 3)*

| mode | model S1 | OC3 | model S2 | DOWEC |
|---|---|---|---|---|
| 1st fore-aft | 0.278 | 0.27 | 0.242 | 0.231 |
| 1st side-side | 0.279 | 0.28 | 0.242 | 0.233 |
| 2nd fore-aft | 1.767 | 2.3 | 1.391 | 1.288 |
| 2nd side-side | 1.836 | 2.4 | 1.424 | 1.376 |

The soil of model S2 consists of a single sand layer for the whole embedment depth. The determination of the linear initial stiffness within the $p$-$y$ model is based on the effective unit weight $\gamma'$, angle of internal friction $\varphi'$ and relative density $D_r$ of the sand, as well as on the pile diameter of the monopile and on the local soil depth. The dataset for the soil parameters is attuned with WP 3 and shown in table 3.

Robustness analysis was used to predict the influence that each of the input parameters has on the natural bending frequencies of the support structure. Some geometry and material parameters were also taken into account with their statistical values as displayed in table 3.

*Table 3: Statistical values of input parameters within robustness analysis for the vibration behaviour of the monopile with soil model S2*

| input parameter | mean value | coefficient of variation | type of distribution |
|---|---|---|---|
| $\gamma'$ | 10 | 0.1 | normal |
| $\varphi'$ | 38 | 0.15 | lognormal |
| $D_r$ | 0.8 | 0.125 | normal |
| Emodul | 2.1E11 | 0.02 | lognormal |
| $\nu$ | 0.3 | 0.03 | lognormal |
| dens | 8500 | 0.01 | normal |
| $th_{tower}^{top}$ | 0.019 | 0.1 | normal |
| $th_{tower}^{bottom}$ | 0.027 | 0.1 | normal |

The statistical dependencies between these input parameters and the natural bending frequencies of the support structure (as output quantities) are carried out using the optimizing structural language optiSLang® [18]. The data for this robustness analysis is obtained from Latin hypercube sampling with 100 samples. In order to predict the intensity of the influence of a single input parameter on the support natural bending frequencies, the COI ("coefficient of importance" [18]) is taken as an indicator (cf. [6]). The variation of the frequency of the first fore-after mode as one outcome of this robustness analysis is shown in figure 6.

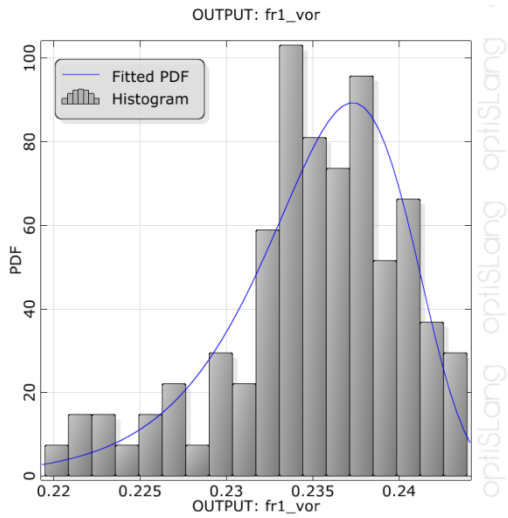


*Figure 6: Fluctuation of the first natural bending frequency (fore-after mode) caused by scattered input parameters*

The results of the other natural bending frequencies are quite similar. The bars in figure 7 indicate how much of the fluctuation in the first support natural bending frequency (fore-after mode) can be explained by a linear relationship to each of the input parameters (table 3). Thereby, the influence of the internal friction angle $\varphi'$ of the soil layer seems to be most dominant, followed by the wall thickness of the bottom of the tower. However, robustness analysis of the investigated model showed that the influences of the chosen input parameters are not significant within this model. So the fluctuations of the natural bending frequencies in the first and second fore-after and side-to-side modes scatter only with few percent of their mean values (see figure 7).

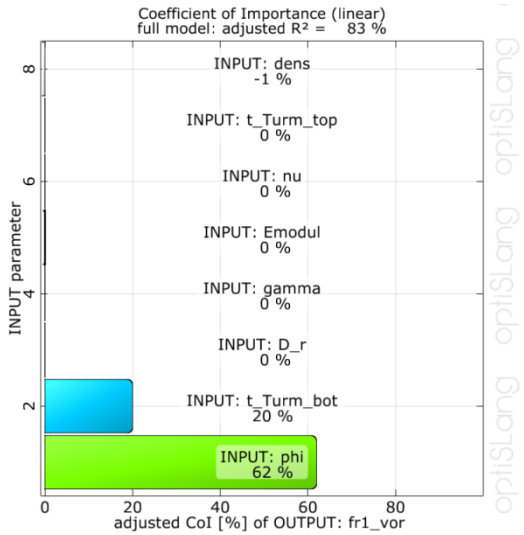


*Figure 7: Linear COIs of the first support natural bending frequency (fore-after mode) with respect to the input parameters (table 3)*

## 2.4.4 Summary and Outlook

During the reporting period, the topics of research were robustness and modal analysis of a monopile as well as the ultimate limit state function of maximum pile resistance for tension loading.

Further development in probabilistic analysis was conducted. For the introduced model of the offshore wind turbine with monopile support structure, modal and robustness analyses were carried out to determine the influences of various model parameters of soil, structure and material on the vibration behaviour of the structure. Different boundary conditions for soil-pile interactions were taken into account within these models and the results were compared to similar investigations of previous reports.

A method was applied to adapt the FINO1 sea-state data to the considered site of the reference offshore wind turbine. Depending on the significant wave height the maximum wave induced pile tension

force was found. In the next step, the ultimate limit state function of the pile resistance for tension loading shall be defined and finalized. The probability of failure will be compared to the limit states as defined in guidelines and standards. Methods shall be proposed to determine the ultimate limit state for other components of jackets and sub-structures in general, respectively.
After the work considering the maximum pile resistance for tension loading is completed, the fatigue limit state shall be considered, using adequate stochastic tools.
Up-to-date, no fully-coupled simulation of wind and wave induced loads has been carried out due to enormous amount of time. The wind turbine and the jacket have been investigated. However, the conditions for a separate investigation shall be determined in order to legitimate this approach.

**References**

[1] Probabilistic Safety Assessment of Offshore Wind Turbines. Annual report 2010, Leibniz Universität Hannover, February 2011.

[2] Probabilistic Safety Assessment of Offshore Wind Turbines. Annual report 2011, Leibniz Universität Hannover, February 2012.

[3] Seidel, M.; Kelma, S.: Stochastic modelling of wind and wave induced loads on jacket piles. Stahlbau, vol. 81, issue 9, pp. 705-710, Ernst&Sohn, Berlin, 2012.

[4] Böker, C.: Load simulation and local dynamics of support structures for offshore wind turbines. Dissertation, Leibniz Universität Hannover, 2009.

[5] American Petroleum Institute: Recommended Practice for Planning, Designing and Constructing Fixed Offshore Platform – Working Stress Design. API (RP2A-WSD), 21st edition, Dallas, 2007.

[6] Goretzka, J.; Rolfes, R.: Modal and Robustness Analysis of the Support Structure of an Offshore Wind Turbine with Scattered Soil Parameters. Proceedings of 8th PhD Seminar on Wind Energy in Europe, ETH Zürich, 2012.

[7] Jonkman, J.; Butterfield, S.; Musial, W. and Scott, G.: Definition of a 5-MW Reference Wind Turbine for Offshore System Development. NREL/TP-500-38060. NREL: Golden, CO, 2009.

[8] Jonkman, J.; Musial, W.: IEA Wind Task 23 Offshore Wind Technology and Deployment – Subtask 2 The Offshore Code Comparison Collaboration (OC3) – Final Report. NREL: Golden, CO, 2010.

[9] Vorpahl, F.; Popko, W.; Kaufer, D.; Description of a basic model of the "Upwind reference jacket" for code comparison in the OC4 project under IEA Wind Annex XXX. Technical Report, Fraunhofer Institute for Wind Energy and Wind System Technology (IWES), 2011.

[10] Coles, S.: An Introduction to Statistical Modeling of Extreme Values. Springer, London, 2001.

[11] Germanischer Llyod: Guideline for the certification of Offshore Wind Turbines. Germanischer Lloyd Industrial Services (GL), Hamburg, June 2005.

[12] IEC 61400-3: Wind turbines - Part 3: Design requirements for offshore wind turbines. Genf, January 2010.

[13] Det Norske Veritas: DNV-OS-J101, Design of Offshore Wind Turbine Structures, Det Norske Veritas (DNV), Høvik, Norway. October 2010.

[14] Dean, R. G.; Dalrymple, R. A.: Water Wave Mechanics for Engineers and Scientists (Advanced Series on Ocean Engineering, Vol. 2). World Scientific Publishing Company, 1990.

[15] Coastal Engineering Research Center: Shore Protection Manual. Washington, 1984.

[16] Mittendorf, K.: Hydromechanical Design Parameters and Design Loads for Offshore Wind Energy Converters. PhD thesis, Leibniz Universität Hannover, 2006.

[17] Kooijman, H.J.T.; Lindenburg, C.; Winkelaar, D. and van der Hooft, E.L.: DOWEC 6 MW Pre-Design: Aero-elastic modeling of the DOWEC 6 MW pre-design in PHATAS. DOWEC-F1W2-HJK-01-046/9 public version. ECN: Petten, 2003.

[18] optiSLang®: Version 3.2.1, opti-SLang Documentation, DYNARDO GmbH, Weimar, Germany, July 2011.

## 2.5 In-Situ Assembly (WP 5)

**Institute of Building Materials Science**
Ludger Lohaus, Michael Werner

### 2.5.1 Motivation

Support structures and turbines of offshore wind turbines (OWTs) are prefabricated segmentally onshore, which offers the possibility of monitoring the production and ensuring the quality. Contrary to this, the foundation and the connection elements between the support structure and the foundation are manufactured under harsh offshore conditions. The gap between pile and sleeve, the so-called grouted joint, is filled with a high-performance mortar called “grout”. These grouted joint connections are used in almost all kinds of offshore structures.

The main problem during the installation process is the application of the grout under offshore conditions [1]. Due to the inaccessibility of the application site, it is difficult to establish an effective quality control to ensure the correct in situ assembly of the grouted-joint connection.

### 2.5.2 Approach

In this work package “supporting structure production in situ”, the risk factors of the grouted joints during the application process will be evaluated taking into account the material behaviour of the grout. Furthermore, concepts used for monitoring and minimising possible defects during execution will also be developed.

The work package is divided into six parts: analysis of common supporting structure types and the positions of grouted joints, analysis of boundary conditions, Preliminary Hazard Analysis (PHA) of the in situ assembly process, Fault Tree Analysis (FTA), and experimental investigations.

The findings of the PHA and the FTA will be used to develop concepts to minimise possible defects, ensure quality control and devise management solutions.

The flow behaviour and the material properties of fresh grout inside the gap between the pile and the sleeve have been unknown until now [2]. This information is important to estimate the effect of failures during the application process. Therefore, a special formwork with a transparent front panel will be constructed to observe the phenomena that occur during and after the pumping process of the grout. Exemplary failure modes will be simulated in this formwork to obtain basic knowledge of the whole situation.

### 2.5.3 State of Work

**Analysis of supporting structure types and influences of the material properties of the grout**

Supporting structures which are used in general are shown in figure 1. The grouted joints are marked with a red circle. The different positions of the grouted joints result from the design of the supporting structure leading to different boundary conditions and different designs of grouted joint. Detailed information is presented in [3]. Furthermore, influences of fresh grout properties are also explained in detail there. The main groups of influences are the grout material itself, the application method, the type of grouted joint construction, and the offshore conditions [3].

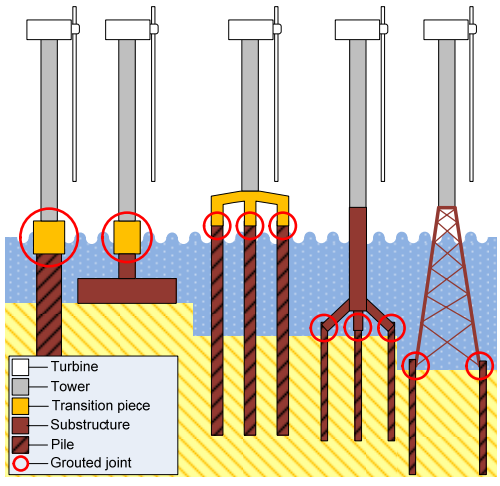


*Figure 1: Supporting structures [3]*

**Grouting procedure**

A functional flow diagram of a typical grouting procedure is shown in figure 2 to find possible failure modes with the help of the PHA. This flow diagram starts with the dry grout material and ends with the hardened grout in the grouted joint.

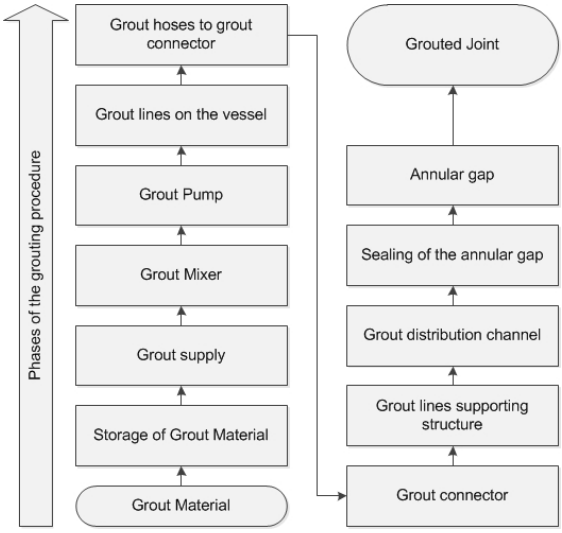


*Figure 2: Functional flow diagram of a grouting procedure*

The dry grout material stored in containers will be supplied in lbig bags by crane to the mixing unit. Then water will be added to the dry material and the ingredients will be mixed by a pan mixer. Another mixing procedure is to use silos with dry grout material and horizontal continuous mixers. After a defined mixing time, the fresh grout will be stored in the storage tank of a grout pump. The freshly mixed grout will then be transported by rubber hoses or steel lines installed on the deck to a transition unit on the ship. From there, the rubber hoses are connected, and supported by crane or by a gangway to a grout connector on the supporting structure. Grout distribution channels reaching to the lower end of the grouted joint are extended from these connector lines of steel or rubber. Fresh grout material will flow into the channel and is distributed among several inlets that lead to the gap between the pile and the sleeve. The material flows downwards on the annular gap sealing, until the inlet point of the distribution channel is reached. The grout will then be pumped upwards until the top of the sleeve is reached.

**Preliminary Hazard Analysis**

The PHA was conducted on the basis of [4], [5] and could be divided into the following five parts which are shown in figure 3. These steps are to conduct a System Design Analysis to find undesired System States, identify failure modes and their effects, evaluate these failures, and recommend corrective actions.

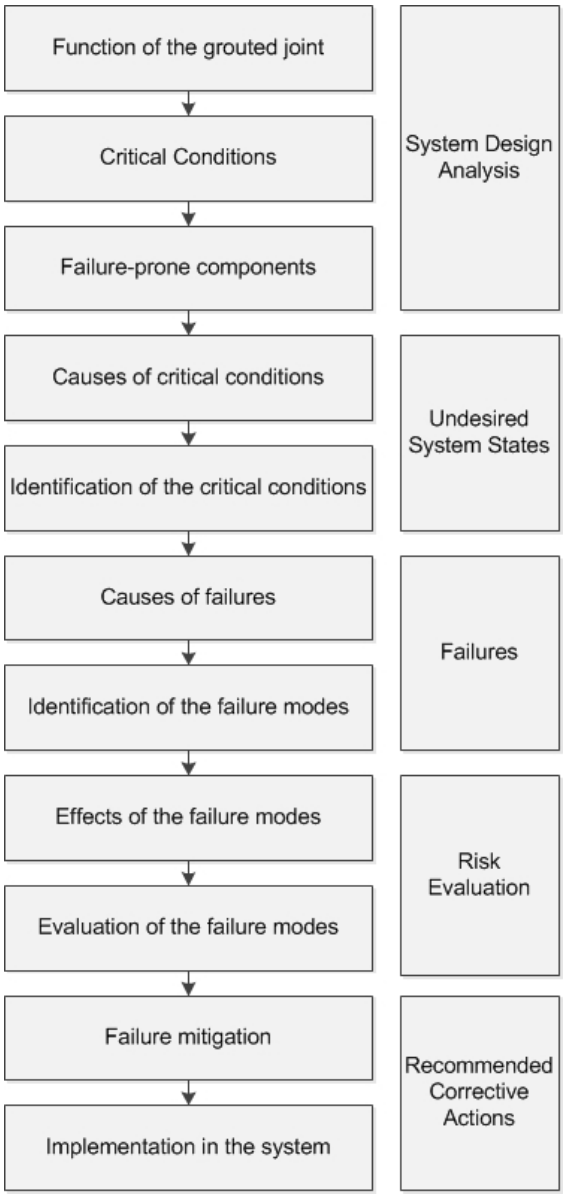


*Figure 3: PHA Process for the in situ assembly*

**System Design Analysis**

The function of the grouted joint is to carry loads from the turbine, tower and supporting structure. These loads are axial loads, vertical loads and also bending moments for monopiles, tripiles and gravity-based foundations. Tripods and jackets are mainly stressed by axial and vertical loads [3].

The cases where the load transfer from the sleeve to the pile is not secured are critical conditions. According to experiences in offshore constructions, the following items are supposed to be critical:

- partially or non-filled gap between the pile and the sleeve, and
- faults in the material in the gap, e.g. voids, insufficient material properties, an insufficient bond between the steel surfaces, and an insufficient bond between the grout and shear keys.

Components which could be failure prone are [6]:

- annular gap,
- sealing of the annular gap,
- distribution channel,
- grout lines which supply the distribution channel, and
- grout connection of the supporting structure.

These prefabricated parts are directly attached to the supporting structure and they are difficult to check after the supporting structure has been placed on the seabed.

The following components will be used on the installation vessel:

- rubber hoses for the grout supply to the supporting structure,
- grout lines on the ship,
- pumping equipment,
- mixing equipment,
- grout material supply, and
- grout material.

Testing and maintenance of these components are more easily possible than the components which are attached to the supporting structure.

**Critical conditions**

Incidents which could lead to critical conditions are irregularities of the grout material, especially of the fresh grout properties, and leakage of the grout seal. Furthermore, a high pump pressure, more time for the grouting procedures than planned and marine fouling in the gap between piles and sleeves could also be critical.

The specific reasons for these incidents could be:

- a fluctuating water demand of the grout material [6];
- irregular size of the grout gap;
- irregular filling of the gap;
- marine fouling of the steel surfaces of the pile and the sleeve;
- minor leakage of the annulus seal;
- rust and impurities in the distribution channel;
- unscheduled mountings of the grout lines to the distribution channel;
- rust, impurities in the grout connector;
- impurities in the rubber hose connected to the supporting structure;
- the running of the lines on the ship;
- impurities in the lines on the ship;
- temperature of the lines, which could have influence on the consistency of the fresh grout;
- extended pumping times because of pumps and mixers with lower capacity; or
- extended time for supplying raw materials by crane because of wind and waves.

**Failures**

Incidents which could lead to failures:

- blocked grout lines;

- massive loss of grout material in the annular gap because of damage to the annular grout seal;
- minimised bond between pile, sleeve and the shear keys;
- grouting procedure outside the specified working time of the grout;
- early age cycling [1]; or
- impact on the structure during the early hardening time.

**Causes of the incidents which could lead to failures**

Blockages of lines and rubber hoses could occur if the lines, the connectors of the lines or the rubber hoses are leaking. Furthermore, the consistency of the fresh grout could have an influence on grout line blockages. If the consistency is too stiff, the friction between the grout and the lines and hoses could become too high. The pump pressure needed could exceed the maximum capacity of the pump and the line gets blocked. If the consistency is too soft, sedimentation of the material in the lines could occur, potentially leading to blockage. Moreover, larger impurities in the lines and hoses, or poor running of the rubber hoses and the lines could cause blockages. Breakdowns of a pump, a mixer or a crane for raw material supply are also possible indirect reasons for a blockage of a grout supply line.

Massive loss of the grout material in the gap between the pile and the sleeve could occur because of damage to the annulus seal. Damage to annulus seals is possible before the grouting process during the placing of the substructure or during the piling process. A loss of the material is possible at the beginning of the grouting process, and also during or at the end of this process due to the exceeding pressure on the seal.

A disturbed bond between the pile and the sleeve could be caused by heavy marine fouling because of a long time period between the placing of the substructure, the piles and the grouting procedure.

A blocked line, or a breakdown of a pump, a mixer [6] or a crane could make the grouting procedure take more time than estimated. Furthermore, the weather conditions could delay the grouting process. Early age cycling may occur because of an unsatisfactory fastening of the pile and the sleeve and also because of heavy waves.

Impact on the hardening grout in the early stage caused by heavy waves, impacts of vessels or by boats on the boat landing could occur.

**Effects of the failure modes**

Consequences of these failures could be as follows:

- The grouted joint is not filled with grout or partly filled; this could be caused by blocked lines or damage to the annulus seal;
- no bond between the surface of the sleeve or no proper bond with the shear keys; this could be caused by marine fouling and also because of early age cycling;
- flaws in the grout or layers with unknown material properties; this could be caused by changing material properties over time;
- planned material properties are not reached because of failures of the mixing proportions, mixing process, storage, and ambivalent temperatures; or
- damage to the grout matrix because of impacts on the structure.

Possible quantifiers of the failure modes are listed below.

The grouted joint is not filled with grout, therefore, no load transfer from the supporting structure to the piles is possible. In this case, a cost intensive rehabilitation may be possible [2]. When the grouted joint is partially filled, further calculations may be possible.

If there is no bond between the surface of the sleeve or no bond between the shear keys and the grout, then the load transfer in the grouted joint is perhaps not so securely based and repair works may be advisable.

If flaws in the grout exist or unknown layers of undefined material properties occur, a concept for monitoring possible movements between the pile and the sleeve may be worthwhile.

When the planned material properties are not reached, a recalculation of the grouted joint could be carried out.

The development of a monitoring concept of a damaged grout matrix may be worthwhile because of possible undefined material properties.

**Examples of failure mitigation**

The following examples of possible measures for the minimisation of failure are reasonable:

- Robust and redundant design of the annulus seal [2];
- adequate dimensions of the distribution channel and the grout lines;
- similar diameters used for grout lines;
- steel lines are better than rubber hoses because of the lower friction between the grout and the line [2];
- carefully planned running of the grout lines and the rubber hoses;
- a redundant grout line system [2];
- emergency plans for possible failures;
- strong fixing of the pile and sleeve to avoid effects from the early age cycling;
- preliminary material test could be conducted under expected conditions;
- mock-up test should be carried out [7] with similar equipment to that used for the grouting operations offshore;
- quality management system for the grout and the grouting process;
- QM system could be audited by external grout surveyors;
- well-trained concrete laboratory technicians with a basic knowledge of grout for grouted joints are perhaps worth using; and
- batches of the grout material chosen could be tested prior to its offshore use.

**Exemplarily implementation of the examples in the system**

- Laboratory test of the grout material, mixing and pumping tests could be carried out in the early design stage of the supporting structure [6].
- Large-scale pumping test could be carried out before the design stage is finished.
- Grout laboratory container could be implemented in the deck layout of the installation vessels with well-trained laboratory staff for self-monitoring.
- External monitoring could be implemented and external material testing [8] for each production batch of the grout material.
- Annulus seal test, leaking tests of the lines and rubber hoses prior to grouting operations [2].
- Equipment tests prior to grouting.
- Documentation of the overflow to check if the annulus seal is leaking and if the grouted joint is completely filled.
- Compressive strength of test specimens under real conditions before the tower and the turbine are connected to the supporting structure.

A Fault Tree Analysis (FTA) will be followed according to the PHA.

**Laboratory testing facility**

A laboratory testing facility was developed to observe phenomena which could occur

during and after the filling of small gaps with grout for grouted joints. New findings by the test facility could prove important for the estimation of failures during the in situ assembly of grouted joints.

A pile with a diameter of 3 m was chosen as a model (figure 4) for the laboratory testing formwork. The grout length of the grouted joint model is 6 m high, and the grouted joint is supplied with grout through four inlets. A scale of 1:4 was chosen for the testing formwork. Furthermore, ¼ of the arc length was chosen for the width of the formwork because of the four inlets in the model of the grouted joint. Hence, the testing formwork will be supplied by one inlet in the middle of the width of the formwork. The front panel is transparent to enable the evaluation of the flow behaviour of the fresh grout. Obstacles, such as shear keys, are fitted on the reverse side of the formwork. The width of the gap is flexible. An attached grout pump is used for the supply with fresh grout. Figure 5 shows the laboratory testing facility.

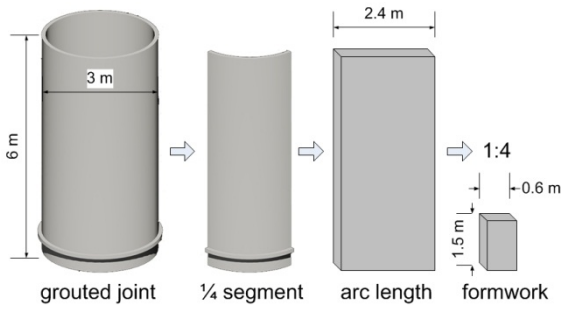


Figure 4: Basic principle of the laboratory testing formwork

The laboratory testing formwork will be filled with two batches of grout and, prior to this, a cement slurry will be used to lubricate the line. After the first batch is pumped into the formwork, a second batch will be mixed and filled after mixing into the formwork. The filling process will be evaluated optically.

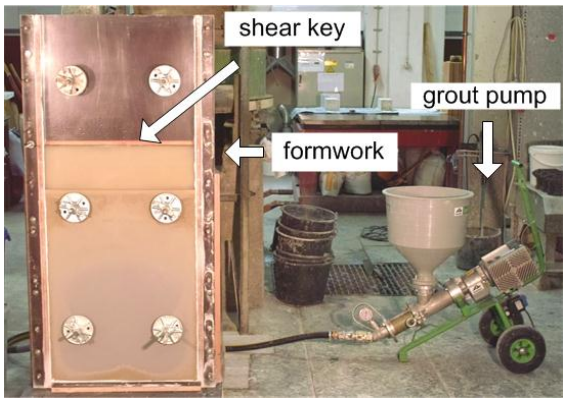


*Figure 5: Laboratory testing facility*

After a period for the hardening of the grout, the sample will be sawed into strips to evaluate whether the grout has sedimented or other phenomena have occurred. Samples of the wall will be taken at several positions to evaluate the compressive and flexural strength of the grout. The results will be compared with test samples according to [9]. A set of three grout samples with the dimensions 40 mm x 40 mm x 160 mm will be used for the comparison.

**First test results**

A standard offshore grout was used for the first two tests. This grout was mixed with a high water content and with a low water content.

The flow behaviour in the grout gap while pumping was self-levelling for both mixtures. The grout flowed without obvious turbulence. Air bubbles passed sporadically in the middle of the gap but continued. The cement slurry settled down to the ground and stayed there till the pumping process of the grout had finished.

After cutting samples out of the wall, the compressive strength was determined. The compressive strength was compared with the standard test samples and the values are seen as percentages in figure 6. A colour scale is situated on the left side which represents 80 percent in red to (and beyond) 100 percent in green.

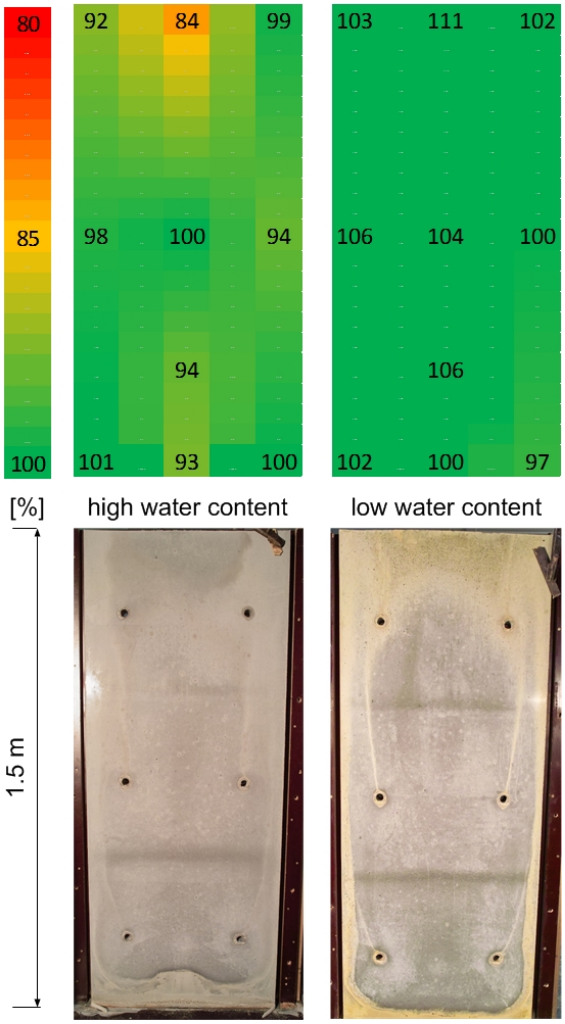


*Figure 6: Results and pictures of the first two test samples*

Test wall 1, which contains the grout with the high water content, is shown on the left side in figure 6. This test wall reached nearly the compressive strength of the standard test samples in most areas of the wall. One area in the middle top area is 16 percent lower than the standard test samples, but the standard deviation of the compressive strength of the wall is low at 6.6 percent.

The compressive strength of test wall 2, which contains the grout with the low water content, is higher than the compressive strength of the standard test samples in all areas of the wall. This wall is a little bit more homogenous with a standard deviation of 4.1 percent.

These first results show that the pumping of offshore grout in the 4 cm gap of the testing formwork had a minor negative effect on the compressive strength of the grout material used. Moreover, the results of the compressive strength of the second trail were higher than the standard test samples. The standard deviations of the compressive strength were also low, hence, this is an indicator for the homogeneity of the material in the gap of the formwork.

**References**

[1] Welham, T.R.; Gilfrin, J.A: „Installation of Grouted Pile-Sleeve Connections: A-state-of-the-Art Review“. 25th Annual OTC, Houston, 1993.

[2] Lohaus, L.; Lindschulte, N.; Scholle, N.; Werner, M.: „Betontechnik für Grouted Joints – Baustoffliche und bauausführungstechnische Anforderungen“. Stahlbau 81(2012), Heft 9.

[3] Lohaus, L.; Werner, M.: „Probabilistic aspects of Offshore Wind Turbines: Influences of in situ assembly of grouted joints“. Life-Cycle and Sustainability of Civil Infrastructure Systems, pp. 2209 - 2213, CRC Press/Balkema, Leiden, The Netherlands, 2013.

[4] Ericson, C., A.: “Hazard Analysis Techniques for System Safety”. John Wiley & Sons, New Jersey, USA, 2005.

[5] Treytl, A.; Himmelbauer, H.: “Fehlerbaumanalyse – Fault Tree Analyses (FTA)”.1996

[6] Lohaus, L.: Offshore-Windenergie A – Design und Installation von Tragstrukturen in der Nordsee (Offshore Windenergieanlagen – Grouted Joints). Fachseminar ForWind, Bremerhaven, September 2012.

[7] Det Norsk Veritas: “Offshore Concrete Structures – DNV OS-C502”. Det Norsk Veritas, Norway, 2012.

[8] Schmidt, M.; Fehling, E.: “Das Gutachten zur Zustimmung im Einzelfall: Konzeption und Inhalt”. Seminar Grouted Joints bei Windkraftanlagen, Kassel, April 2011.

[9] DAfStb-Richtlinie: Herstellung und Verwendung von zementgebundenem Vergussbeton und Vergussmörteln. Beuth Verlag, Berlin, November 2011.

## 2.6 Monitoring of Mechanical Components (WP 6)

**IMKT (Institute for Machine Design and Tribology)**
Gerhard Poll, Roman Böttcher

The number of installed wind turbines grows dramatically as well as the power of newly developed turbines in light of the turnaround in energy politics towards renewable energies. In addition, there is an increasing number of wind turbines installed or planned to be installed in near and far offshore conditions. Offshore wind turbines (OWT) are normally supposed to have the same reliability as turbines on land although they are more difficult to access which results in a longer downtime in case of a failure that has to be repaired.
Damages in the mechanical drive train of wind turbines cannot be determined and excluded in advance sufficiently. The aim of work package 6 therefore is the development and optimization of monitoring and diagnosis systems that should be applicable to OWT to provide reliable operation and efficient maintenance through early detection of damages and force monitoring. It also helps to achieve basic knowledge during experimental studies on single components of the OWT drive train.

### 2.6.1 Motivation

The largest part of operation costs for onshore wind turbines are maintenance costs as pictured in the table below.

| Onshore Wind | Share of Operation and Maintenance Costs (%) |
|---|---|
| Maintenance (service and spare parts) | 26 % |
| Administration | 21 % |
| Land rent | 18 % |
| Insurance | 13 % |
| Power from the grid | 5% |
| Other costs | 17% |

*Table 1: Breakdown of Operation and Maintenance Cost for Onshore Wind [2]*

Offshore wind turbines are naturally less well accessible then onshore turbine because of their location in open water. In addition maintenance and repair are made more difficult due to the fact that the turbines aren't accessible by ship for over half of the year because of critical wave heights above 1m, see [1] for measured sea state in the German Bight for 2011. Therefore, losses as a consequence of a longer response time and thus of more downtime in the event of failures are accompanied by higher costs for transport of material and staff for repair by ship or even helicopter. For this reason, maintenance costs have a larger share on the operation costs of OWTs compared to the composition of expenses for operation of onshore turbines, see table 2. More effective planning of maintenance and the prevention of damages in the drive train of OWT can therefore help to reduce operation costs.

| Offshore Wind | Share of Operation and Maintenance Costs (%) |
|---|---|
| Maintenance (service and spare parts) | 39 % |
| Port activities | 31 % |
| Operation | 16 % |
| License fees | 3 % |
| Other costs | 12 % |

*Table 2: Breakdown of Operation and Maintenance Cost for Offshore Wind [2]*

**Lifetime of Rolling Element Bearings in Wind Turbines**

All mechanical components in the drive train of OWTs are subjected to forces and speeds resulting from the impact of a permanently changing wind on the rotor as well as events on the electric end of the system e.g. short circuits. Malfunctions of rolling element bearings due to fatigue as a result of repetitive overrolling occur even under ideal lubrication conditions and are typically distributed stochastically. For the dimensioning of bearings, a failure probability can be calculated. Dynamic loads can be approached by histograms with a finite number of simplified static values. Thereby, short time events, e.g. wind gusts on the wind side or short

circuits on the electric side of a wind turbine cannot be taken into account as well as the sequence of the load distribution when calculating over an estimated life time of a turbine of 20 years. The influence of short time events on the lifetime of cylindrical roller bearings (CRB) was investigated during a research project at IMKT, see also [3]. As a result, short time events cannot be considered as causal for frequent failures in gear boxes of wind turbines. Endurance tests with different load steps even showed an increasing lifetime, when CRBs were exposed to initial high loads before testing with normal loads.

Non-stationary loads induce additionally particular effects, such as slip of rolling elements and subsequent smearing damages that can reduce the lifetime of bearings in wind turbines. Slip of rolling elements is defined as a divergence of their actual movement to the motion predetermined by their geometry. Three slip conditions can be distinguished as shown in fig. 1. Lateral slip can occur due to tilting in CRBs or due to dynamic axial loads that displace the bearing parts in its axial clearance repeatedly.

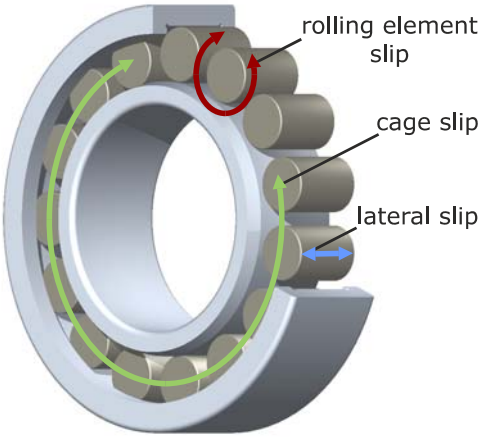


*Figure 1: slip in rolling element bearings*

Slippage in circumferential direction of both rolling elements and cage respectively the whole rolling element set results from rotational accelerations of the bearing while the forces in the contact of rolling elements and their raceways aren't sufficient high enough to ensure a pure rolling motion. The risk of slip increases with growing bearing dimensions on account of an increasing mass-inertia of the bearing parts. As a consequence, an oversizing of rolling element bearings is not reasonable to ensure higher lifetimes. Large size bearings of wind turbines are especially endangered to endure slippage by reason of their dimensions and non-stationary and non-controllable operation conditions. The influence of slippage, as long as it did not already caused visible wear, on the lifetime of rolling element bearings is not yet investigated sufficiently and therefore not even implemented in their lifetime prediction.

**Condition Monitoring of Bearings in Wind Turbines**

Condition monitoring systems (CMS) are already used in other industries to detect failures and to control e.g. power plants, paper machines and rolling mills. CMS for wind applications can monitor different parts of a wind turbine, e.g. rotating bearings, gears, generator coils, the integrity of rotor blades and structural components or parts of the power electronic. CMS for mechanical parts of wind power plants can be certified by Germanischer Lloyd, see [4], and are acknowledged by different insurance companies.

Since the lifetime of rolling element bearings in wind turbines isn't predictable satisfactorily as shown in the prior paragraph, supervision systems need to be developed that ensure an early detection of inevitable damages and a rapid response of the control of the wind turbine. By help of CMS that monitor vibration signals of bearings in wind turbine gear boxes, expensive secondary damages on other mechanical components, such as gears or other bearings, and therefore longer downtimes can be avoided as long as the turbine is turned down before the bearing damage increases and particles get in contact with

other components. With knowledge of the damage progress in rolling element bearings, wind turbines even could be operated to the next scheduled maintenance with reduced load after damages occur. Downtime could be minimized further which leads to an increasing current efficiency. This applies particular to OWTs as already described.

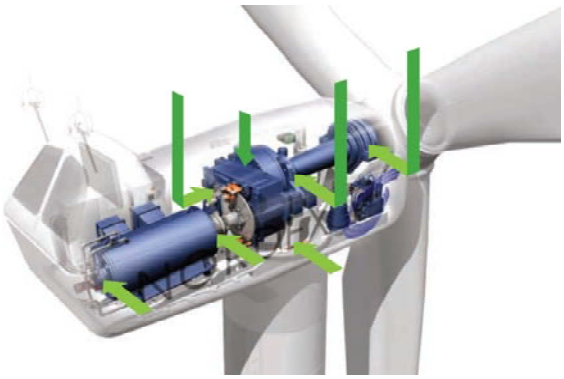

*Figure 2: minimum number of sensors [5]*

Damages in the raceways of rolling element bearings produce a shock pulse repetition when rolled over repeatedly. The frequency of the pulse repetition depends on the geometry of the bearing, damage location (inner ring, outer ring, cage or rolling element) and the rotational speed.
To detect pulse shocks of damages in the best possible way, acceleration sensors have to be mounted in load direction and as close as possible to the specific bearing and its loaded zone. However, several bearings can be monitored by only one sensor in practice by taking advantage of transmission properties of structural components. The particular mounting position of vibration pick-ups has to be selected carefully with regard to transmission behavior at all desired frequencies. The certification guideline of Germanischer Lloyd for CMS in wind turbines demands at least six acceleration sensors on main shaft, gearbox and generator, [4]. Figure 2 shows an actual approach with seven sensors, which are mounted both radially and axially, at different parts of the drive train of a wind turbine.

This vibrational signal cannot be analyzed directly because of an amplitude modulation with other vibrations with higher frequencies which result e.g. from structural vibrations, tooth meshing frequencies or additional components for operation. Current condition-monitoring-devices use low-pass-filters to separate an envelope curve with the interesting part of the signal. Cut-off frequency, filter type and order of the filter have to be adapted for different rotational speeds and every gearbox. This approach requires that the modulated vibrations and the transmission behavior of the structural components do not vary during operation and life time of the wind turbine. The envelope curve produced by filtering can be distorted due to transient response or overshoots.
The envelope curve has to be transferred to a frequency spectrum by help of FFT, where amplitudes of characteristic overrolling frequencies can be evaluated to detect damages. Depending on the movement of the bearing parts, harmonics show up in the frequency spectrum as well.
While operating with variable speed, the original vibration signal can be frequency modulated additionally. This influence can be removed by use of order tracking analysis instead of frequency spectrums.

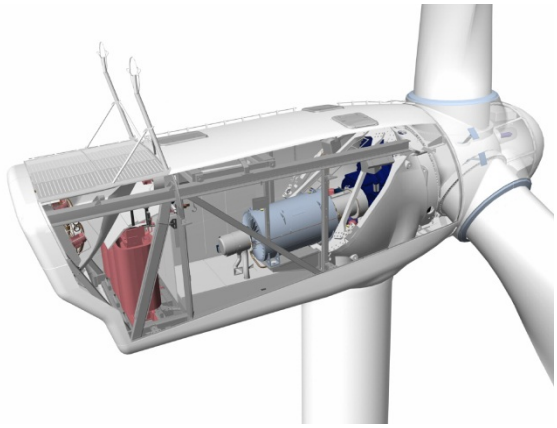

*Figure 3: integrated drive train [6]*

The design of drive trains in wind turbines changes with increasing size and power. In partly integrated designs as shown in

figure 2, one bearing of the rotor is integrated into the gearbox. To reduce the tower head mass, integrated drive trains were developed, where rotor and gear box as well as gear box and generator are connected directly without the use of intermediate shafts. Therefore, more rotating parts emit vibration signals in the housing of the gearbox, making it less easy to separate certain pulse shocks.
Further space savings and higher gear ratios for slower rotating rotors could be achieved by substitution of spur gears with planetary gears. Since planet wheels rotate around themself and rotate with their carrier, shock pulses of damages in planetary bearings are difficult to detect with stationary acceleration sensors and conventional CMS-methods.

## 2.6.2 Approach

For A new type of analysis procedure as described in [7] shall be examined in conjunction with novel acceleration sensors to prevent causes of error in the detection of bearing damages as a result of the difficulties as described in the previous chapter (variable speed, filter design, more compact drive trains). This method uses a Hilbert transformation to get an envelope curve without the usage of filters. By early detection of fatigue in rolling element bearings and knowledge of effective loads during operation, further understanding regarding the mechanism of bearing damages can be achieved. Therefore sensors to monitor loads on components of OWT have to be examined as well.

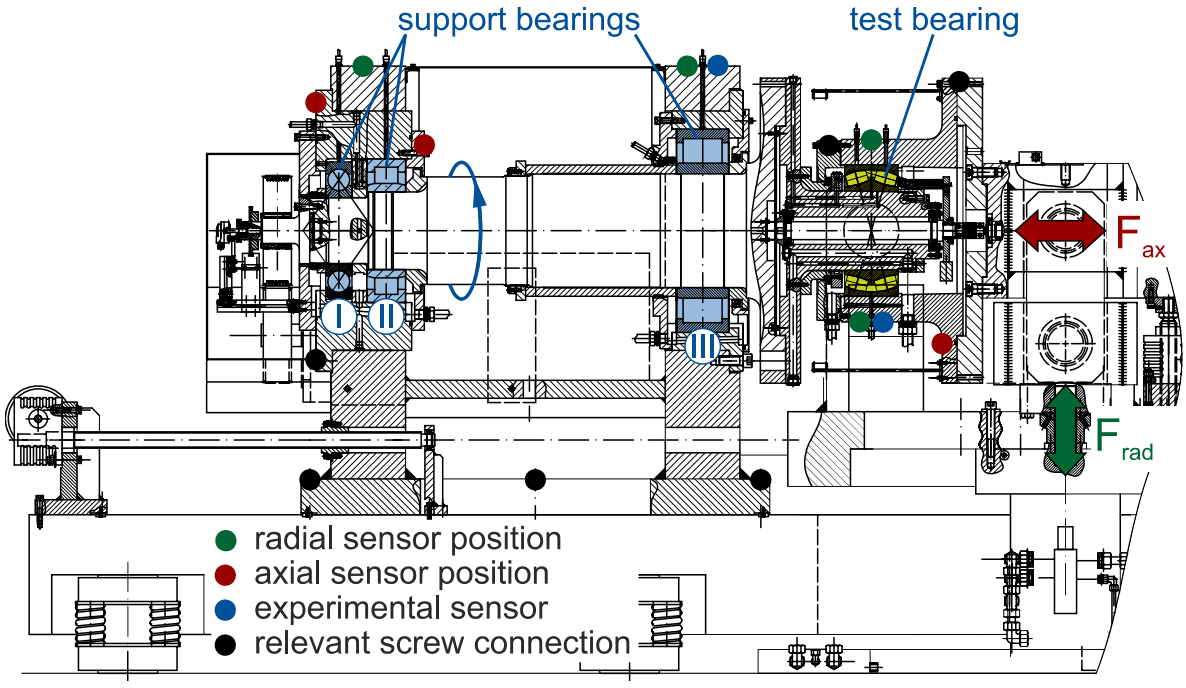


*Figure 4: Large size bearing test rig, setup for rotating inner ring*

For experimental investigations with large size bearings under various conditions, especially those that may cause unexpected bearing damages or failures in practical applications, a large size bearing test rig is at IMKT's disposal. Fatigue life of small bearings with different loads and speeds can be tested at several small test rigs at IMKT.

**Condition Monitoring System**

The novel procedure of analysis was already tested successfully on a test rig for small CRBs with constant load and rotational speed, see [7]. As already mentioned, the conditions in OWTs impose special requirements. Therefore, the CMS shall be tested and developed under operation conditions which are

similar to OWTs on the large size bearing test rig as shown in figure 4.
The bearing test rig for large size bearings consists of a single test bearing and also two cylindrical roller bearings and one radially relieved four point bearing as support bearings. The axial and radial load as well as tilting can be applied by means of hydraulic cylinders both in tension as well as in compression. In addition the test bearing can be operated optionally with a rotating inner or a rotating outer ring.
Figure 4 shows all accessible positions on which acceleration sensors were mounted on the large size bearing test rig to cover as many loaded zones of each bearing as possible. The plotted curves in figure 5 represent added up amplitudes of the characteristic overrolling frequencies and their harmonics of both inner and outer ring of the test bearing. The related vibration signal was recorded during scheduled non-continues investigations over several weeks with different operation conditions by an accelerometer on the housing of the large CRB, marked as III in figure 4. An increasing in the characteristic value could be observed. After dismounting, the test bearing showed indentations from particles in its raceways.

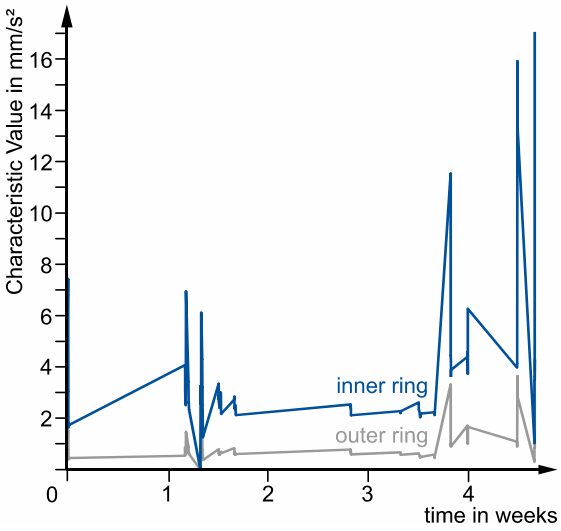


*Figure 5: Envelope curve trend of a test bearing at the large size bearing rig*

In addition to commercial acceleration transducers that utilize shear of a piezoceramic by a seismic mass to measure vibration signals, experimental sensors were bonded to the test rig in direct vicinity to proven sensors. These sensors require less space and are lighter than their traditional counter parts. While the latter have integrated electronic components to convert a charge, generated by a deformation of the piezo-ceramic, to an output voltage, a detached amplifier has to be used for the experimental sensors. First simple tests show a good performance.

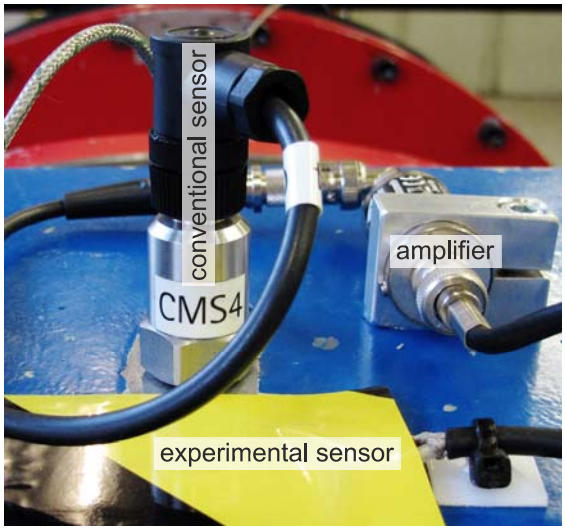


*Figure 6: Amplifier and experimental vibration pick-up*

**Preload of screw connections**

Since most of the bearings in gearboxes of wind turbines are carried by housing parts that are bolted together, actual forces on bearings could be examined by measuring of preload forces in screw connections. Different sensory washers that enable the measurement of preload forces can be already purchased. These sensors use either strain gauges or piezoceramics. Both measurement principles have characteristics that are not compatible with one of the following requirements for this particular application in OWT:

- measurement of both static and axial loads
- retrofitable
- durable

- simple design
- no influence on the stiffness of screw connections

To match all requirements listed above, new sensors are developed by Frauenhofer IST from Braunschweig, see [8], and DLR in Cologne. These sensors consist of microstructured layers on a steel substrate, as shown in figure 7, to take advantage of the piezoresistive effect as described first in [9]. The sensor layer based on diamond-like-carbon (DLC) allows to measure forces without significant deformations in contrast to strain gauges.

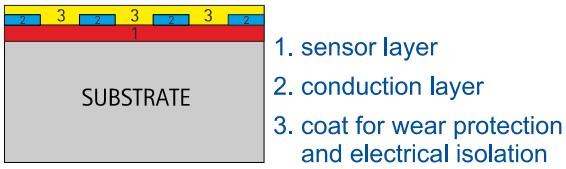


*Figure 7: Schematic configuration of a piezoresistive sensor*

To evaluate characteristics of these novel sensors, e.g. transmission behavior, influence of temperature and drift, static tests shall be performed in a lifetime test rig for smaller bearings. Afterwards the sensor shall be applied to the large size bearing test rig to measure forces under dynamic conditions similar to those in OWT. Relevant screw connections on the large size bearing test rig are indicated in figure 4. Some of them lay in direct flux of test force while the variation of the preload force due to test forces is also affected by friction between components on other screw connections.

## 2.6.3 State of Work

### Condition monitoring system

The described condition monitoring system is installed at the large size bearing test rig for adjustment and testing under defined operation conditions during run-ups and scheduled experimental investigations. All sensors as shown in figure 4 are mounted. It has to be figured out which sensors are necessary for future investigations since the hardware for data acquisition is currently limited to seven input channels with sufficiently sampling rate.

The large size bearing test rig is not intended for durability tests with bearings. Therefore, fatigue damages on one of the bearings are not supposed to occur during scheduled tests. To nonetheless gain knowledge about characteristic values of the vibration levels of damage frequencies, a test bearing will be damaged in a defined way. A suitable test bearing was already acquired and mounted.

Two experimental vibration pick-ups were already tested by applying impacts to the structure of the rig. Methodical investigations have to be performed to detect the influence of temperature and electrical interference. In addition the resistance to typical lubricants of bearings in gearboxes of OWT has to be examined since the sensors are supposed to work inside the gearbox, too.

### Preload of screw connections

A test rig for smaller bearings was already redesigned to test the sensors under static conditions during a student research project. The application is still pending since no sensor could be purchased until yet. A new attempt will be made in the beginning of 2013 when new results are expected.

**References**

[1] Federal Maritime and Hydrographic Agency: Sea State for 2011, http://www.bsh.de/de/Meeresdaten/Beobachtungen/Seegang/S2011/Netz.jsp, Nov. 2012.

[2] Arapogianni, A.; Moccia, J.: Economics of Wind Energy, Modern Energy Review, Vol. 4, Issue 2, 2012.

[3] Hacke, Radnai, Hinkelmann; Berücksichtigung von Betriebszuständen, Sonderereignissen und Überlasten bei der Berechnung der Wälzlager-Lebensdauer in Windenergieanlagen und Großgetrieben; Abschlussbericht FVA 541; Forschungsvereinigung Antriebstechnik e. V.; 2010.

[4] Guideline for the Certification of Condition Monitoring Systems for Wind Turbines, Edition 2007, GL Renewables Certification guidelines.

[5] Becker, E.: Measuremnet locations and diagnostics in WPPs, tele-diagnose.com (magazine), No. 05, September 2003.

[6] German Wind Energy Associatiom: http://www.wind-energie.de/sites/default/files/images/page/2011/maschinenhaus-antriebstrang/5-16-teilintegrierte-triebstrangskette-nordex-n54.jpg, Nov. 2012.

[7] Hacke, B.; Früherkennung von Wälzlagerschäden in drehzahlvariablen Windgetrieben, Phd. Thesis, Verlag Dr. Hut, 2011

[8] Biel, S.; Lüthje, H.; Bandorf, R.; Sick; J.-H.: Multifunctional thin film sensors based on amorphous diamond-like carbon for use in tribological applications, Thin Solid Films, vol. 505, issue 3, 2006, p. 1171–1175

[9] Pfann, W. G.; Thurston, R. N.: Semiconducting stress transducers utilizing the transverse and shear piezoresistance effects," Journal of Applied Physics, vol. 32, no. 10, p. 2008, 1961.

## 2.7 Diagnostic Systems for Electronic Systems (WP 7)

**Institute of Drive Systems and Power Electronics**
Meike Wehner

### 2.7.1 Motivation

Faults and defects in electrical machines, such as winding faults, short-circuit faults or rotor eccentricities, result in characteristical changes of the magnetic air-gap field, whose dependency on position and time was investigated in previous works at IAL-AS.
Using sensors such as search coils, the local dependence acts as a filter supporting the detection of a fault or defect with high signal-to-noise ratio as well as the identification of the type of fault by signal frequency.
In theory, the sensor signals are assumed to be zero in faultless wind generators. In industrial applications, the signal fluctuation as well as the reachable signal-to-noise ratio have to be evaluated. On the other hand, the influence of the generator type and the power electronic components concerning reliability has to be researched.

For this reason, two diagnostic systems will be dimensioned and realized in prototypes. Finally, the measured data are evaluated, and based in this, appropriate design criteria are elaborated for this kind of diagnostic systems.

For the application in wind energy plants, three generator types are in common use. Besides doubly-fed induction machines and salient pole synchronous machines, permanent magnet synchronous machines have been used more and more during the last years. In a first step, a search coil system for 4-pole doubly-fed induction machines shall be dimensioned. The resulting air-gap field and the voltages induced in case of a fault are analyzed based on rotating field theory by using the software ALFRED, which has been developed at IAL.

### 2.7.2 State of Work

Fault detection is made by using characteristical changes of the electromagnetic air-gap field. In [1,2,3,4], comprehensive investigations have been made concerning the appropriate arrangement of search coils in air gaps. In [5], dimensioning of the search coil system for a doubly-fed synchronous generator with $2\mathrm{p} = 4$ poles and $\mathrm{N}_1 = 72$ stator slots is made. The results of consideration are presented below.

Dimensioning of search coil systems can only be done optimally for a spatial harmonic field of one chosen number of pole pairs. As this reference number of pole pairs, $\nu_R = p - 1$ is selected, as it will be produced in case of all investigated failures (winding faults and rotor eccentricities).
As a compromise between the number of conductors of the search coil system and the selectivity, a two-slot winding is selected with the shift $\tau = 12$ respectively between forward and return conductor.

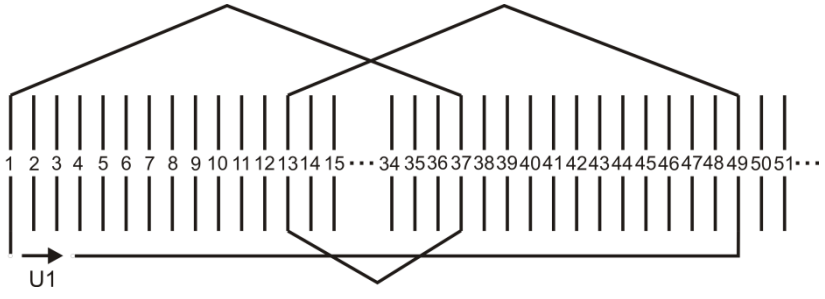


*Figure 1: Winding distribution of search coil system in stator slots*

The width of search coils is $W_m = 36$ stator slots. The search coil distribution in the stator slots is shown in figure 1.

By using only one search coil system, the induced voltage in the search coils depends on its arbitrary location between fault location and coil system. In order to avoid this local dependence, a second identical search coil system is used, shifted towards the first one along the circumference.
This 2-phase search coil system allows separating the voltage components induced from two rotating spatial harmonic fields with equal reference number of poles and frequency but different directions of rotation. Here, the positive-sequence component (index m) has the same direction of rotation as the primary field, the negative-sequence component has the reverse rotating direction (index g). The voltages $U_m$ and $U_g$ are named as symmetrical components of the voltage. A zero-sequence voltage does not exist in a 2-phase system.

Several faults are analysed by using the software ALFRED, which has been developed at IAL. In accordance with the mathematical derivations [3] and based on the rotating field theory, the software determines the resulting air-gap field as well as the voltages induced in the search coil system.

Using the search coil system dimensioned before, it is shown in [5] and [6] that winding faults, static and dynamic eccentricities can be identified for the simulated wind generator, based on the frequency components of the induced voltage which are characteristic for the type of fault.

**Signal-to-noise Ratio**

In theory, no voltage is induced in the search coil system of a faultless generator. In practice however, also in faultless mode eccentricities, e.g. due to shaft bending or inaccuracies during assembly, cannot be avoided and, consequently, voltages are induced in the search coils even without fault. For this reason, further analysis is needed, in how far the detection of faults will be influenced by existing residual eccentricities.

In [6], the effect of an existing static eccentricity on the detection of a winding fault was determined. For both failures, the characteristic frequency of the induced voltage is the line frequency. In case of a static eccentricity however, the induced voltage has negligible negative-sequence component at line frequency, which hereby is a good indicator for the detection of winding faults with high signal-to-noise ratio, as shown in figure 2.

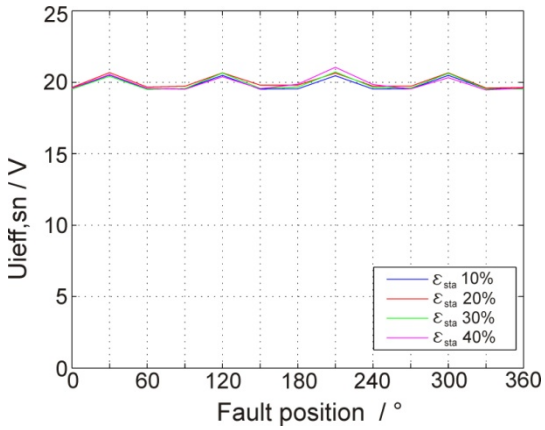


*Figure 2: Signal-to-noise ratio of negative-sequence component of induced voltage for a winding fault with static eccentricity*

Next, the effect of an existing dynamic eccentricity on the voltage induced in the search coils in case of an occurring winding fault was examined. The dynamic eccentricity was assumed with $\epsilon_{dyn} = 20\,\%$ and a fault location of $\varphi_{dyn} = 30\,\%$, the short-circuit current with $I_{FE} = 1000$ A. The indicator for a dynamic eccentricity is an induced frequency of

$$f = f_1 \{1 - \frac{1}{p}(1 - s)\}, \qquad (1)$$

which results in a characteristical frequency of 25 Hz for the simulated generator, there is no effect on the detection of an occurring winding fault. Figures 3 - 5 show the frequency analysis

of induced voltage of winding fault and dynamic eccentricity on its own, as well as for a winding fault with existing dynamic eccentricity.

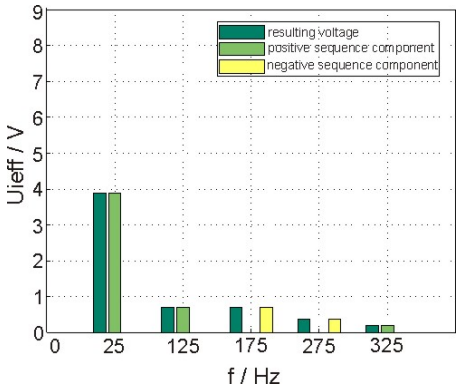


*Figure 3: Frequency analysis of induced voltage for a dynamic eccentricity of $\epsilon_{\mathrm{dyn}}$ = 20 % and $\varphi_{\mathrm{dyn}}$ = 30 °*

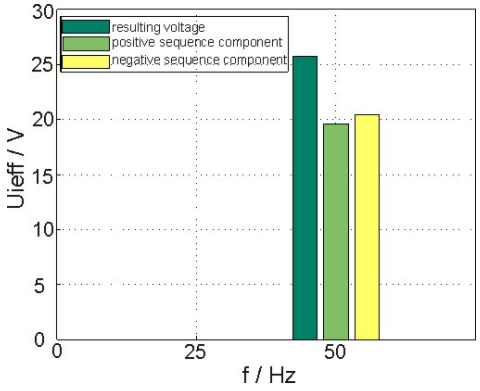


*Figure 4: Frequency analysis of induced voltage for a winding fault with $I_{FE}$ = 1000* A

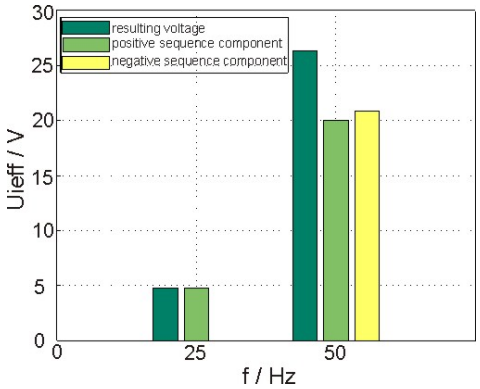


*Figure 5: Frequency analysis of induced voltage for a winding fault with $I_{FE}$ = 1000 A and an existing dynamic ec-centricity of $\epsilon_{\mathrm{dyn}}$ = 20 % and $\varphi_{\mathrm{dyn}}$ = 30 °*

The difference between the characteristical frequencies also simplifies the detection of an occurring dynamic eccentricity with existing static eccentricity and vice versa. As seen in figure 6, a static eccentricity results in frequencies of induced voltage with line frequency and uneven multiples of line frequency. Hence the measuring-relevant frequencies of both kinds of eccentricities are not influenced by each other and both failures can be detected with high signal-to-noise ratio. The frequency analysis of combined static and dynamic eccentricity is shown in figure 7.

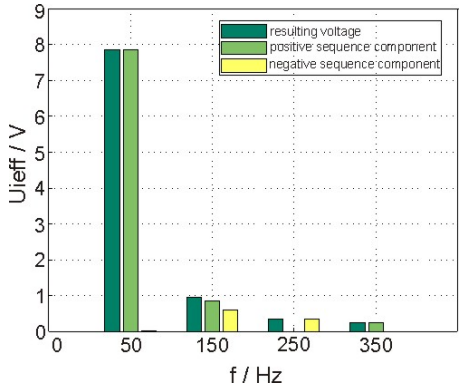


*Figure 6: Frequency analysis of induced voltage for a static eccentricity of $\epsilon_{sta}$ = 20 % and $\varphi_{sta}$ = 30°*

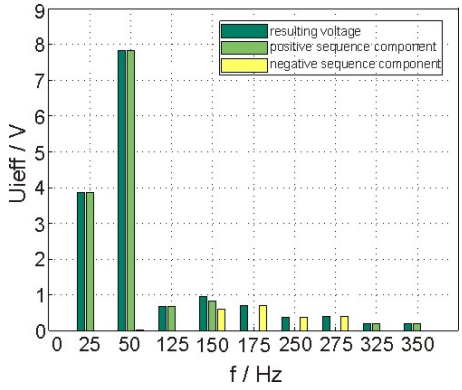


*Figure 7: Frequency analysis of induced voltage for a dynamic eccentricity of $\epsilon_{dyn}$ = 20 % and $\varphi_{dyn}$ = 30 ° and an existing static eccentricity of $\epsilon_{sta}$ = 20 % and $\varphi_{sta}$ = 30 °*

**Conclusion**

Using the search coil system dimensioned before, it was determined, in how far the detection of faults will be influenced by existing static or dynamic eccentricities. In case of an existing static eccentricity, winding faults can be detected by the evaluation of the negative-sequence component of line frequency. As dynamic eccentricities result in a different characteristical frequency than winding faults and static eccentricities, the detection of these faults is not affected by an existing dynamic eccentricity.

**References**

[1] Pittius, E.; Analytische und Experimentelle Behandlung von Erdschlüssen in Asynchronmaschinen. Dissertation an der Universität Hannover, 1989. Fortschritt-Berichte VDI, Reihe 21, Nr. 48

[2] Früchtenicht, S.; Analytische und Experimentelle Behandlung von Wicklungsschlüssen in Asynchron-maschinen. Dissertation an der Universität Hannover, 1990. Fortschritt-Berichte VDI, Reihe 21, Nr. 56

[3] Ponick, B.; Fehlerdiagnose bei Synchronmaschinen. Dissertation an der Universität Hannover, 1994.

[4] Seinsch, O.; Rust, S.; Überwachung von Windungsschlüssen im Läufer von Induktionsmotoren mit Schleifringläufer, Elektrie, Berlin 50, 1996

[5] Wehner, M; Probabilistic Safety Assesment of Offshore Wind Turbines, WP 7, Annual Report 2010

[6] Wehner, M; Probabilistic Safety Assesment of Offshore Wind Turbines, WP 7, Annual Report 2011

## 2.8 Reliability of the Grid Connection (WP 8)

**Institute for Drive Systems and Power Electronics (IAL)**
Felix Fuchs

**Institute of Electric Power Systems (IEE)**
Stefan Brenner

Regarding the probabilistic safety of offshore wind turbines, the electrical system and the grid connection cannot be neglected. Together with work package 6 and 7, mechanical and electrical examination is covered.
The work package 8 is a collaboration between the Institute for Drive Systems and Power Electronics and the Institute of Electric Power Systems. The overall aim is to evaluate different grid connection topologies from the probabilistic point of view concerning the reliability. The two mentioned institutes are on the one hand specialized in the generator and its frequency converter and on the other hand in the grid connection itself.
The probabilistic reliability model of the whole electrical system will be implemented by the Institute of Power Systems, while the Institute for Drive Systems and Power Electronics delivers reliability models for power electronics and filter elements within the grid connection.

### 2.8.1 Motivation (IAL)

In the field of electrical power supply the reliability of the system plays an important role. For the investor the breakdown of a wind turbine always means losses by reason of costs of repair and loss of (financial) compensation for electricity fed into the grid. Especially in the field of offshore wind parks a breakdown leads inevitably to long down times, because repairing takes longer due to limited accessability. In figure 1 it can be seen, that the higher the power of the wind turbines is, the more often the electrical part of the system fails. It is thus most important to investigate the reliability of the electrical system of large (offshore) wind turbines and their grid connection. The wind as a stochastic factor is an important input factor that determines load cycles and stress of the wind turbine. This gives also a motivation to examine the system from a probabilistic point of view.

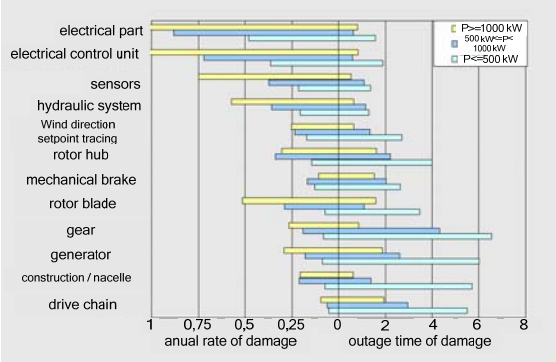


*Figure 5: Frequency of damage and corresponding outage time of wind power plants sorted by components for different output power (from [1])*

### 2.8.2 Approach (IAL)

In figure 2, the topology of an offshore wind park, its internal interconnection and its connection to the onshore grid can be seen.

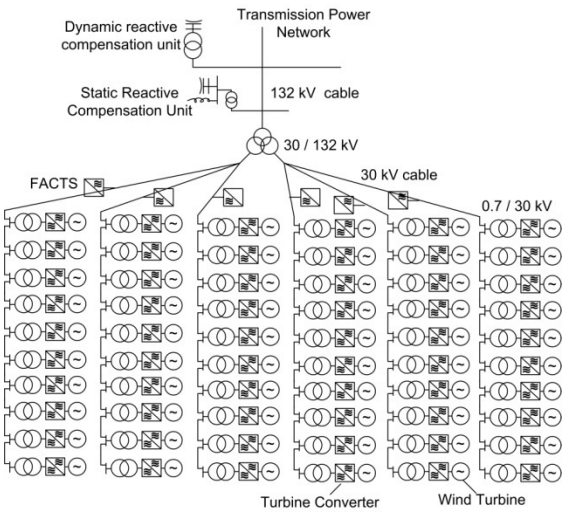


*Figure 6: Example of the grid connection of an offshore wind park (in part from [2]).*

Each wind turbine has a frequency converter, filters and a step up transformer. Other frequency converters

could control the power flow within the offshore grid (FACTS). Another step up transformer (30 kV /132 kV) gives the high voltage for transmitting the power through a sea cable to an onshore grid connection point. Compensation units (reactive compensation) help controlling the power flow. An alternative way to transmit the power onshore is a high voltage DC (HVDC) connection.

This overall system is in the focus of work package 8. All parts of the offshore grid concerning power electronics (frequency converters) and filters (capacitors, chokes) are covered by the Institute for Drive Systems and Power Electronics. Models giving information about their failure performance will be built. It is the aim to get a probabilistic model for the whole grid connection for computing the reliability. This will be done by the Institute of Electric Power Systems.

## 2.8.3 State of Work (IAL)

From the point of view of the Institute for Drive Systems and Power Electronics, at first, the focus of the project lies on the frequency converter of an offshore wind turbine. In further steps, other frequency converters and filter elements will be considered. Weak elements of the power transmission chain in a wind turbine are the power semiconductor modules of the frequency converter [3]. So, the first aim is to get a probabilistic reliability model for the failure of the power semiconductors of the converter. In offshore wind turbines, mainly two topologies of generator-converter systems exist: The doubly-fed induction generator (DFIG) and the permanent magnet synchronous generator (PMSG). Both will be analyzed in this project.

The influence of operation statistics on the lifetime of power semiconductor modules in DFIG was investigated first. The most important factor influencing their lifetime is the varying junction temperature [3]. The junction temperature is dependent on the power flowing through the converter. With the software Matlab/Simulink/PLECS, it is possible to simulate the junction temperature variation of the power semiconductors. As it can be seen in the annual report 2011, at first a stationary model of the system was built and analysed. In 2012, a dynamic model of a DFIG wind turbine was realized to get the dynamic thermal load of the power semiconductors in the converter. This will be described in the following.

Mechanical Modeling of a 2 MW DFIG wind turbine

The first aim is to find a suitable power characteristic ($c_p$-characteristic). Several characteristics are found in literature. They are described by the following equations:

$$c_p(\lambda,\beta) = c_1\left(\frac{c_2}{\lambda_i} - c_3\beta - c_4\beta^{c_5} - c_6\right)e^{-\frac{c_7}{\lambda_i}} \quad (1)$$

$$\frac{1}{\lambda_i} = \frac{1}{\lambda + c_8\beta} - \frac{c_9}{\beta^3 + 1} \quad (2)$$

Here, $\lambda$ is the tip speed ratio and $\beta$ is the pitch angle. The coefficients $c_i$ are given in table 1. For configuration 6, the following equation holds:

$$c_{p,GE}(\lambda,\beta) = \sum_{i=0}^{4}\sum_{j=0}^{4}\alpha_{i,j}\beta^i\lambda^j \quad (3)$$

The characteristics are plotted versus the tip speed ratio λ in figure 3. Table 1 shows their characteristics.

*Table 1: Cp Curve Properties*

| Configuration | $\lambda_{opt}$ | $c_{pmax}$ | $c_p$ drop from 0° to 5° |
|---|---|---|---|
| (1) | 8.9 | 0.4176 | ~91% |
| (2) | 4.95 | 0.4332 | ~87% |
| (3) | 8 | 0.4109 | ~69% |
| (4) | 7.2 | 0.438 | ~69% |
| (5) | 6.2 | 0.44 | ~80% |
| (6) | 8.8 | 0.52 | ~71% |

Concerning the speed control, only configuration 1 was found to be suitable for the 2 MW wind turbine [4]. The

corresponding pitch angle reference for full load is shown in figure 3.

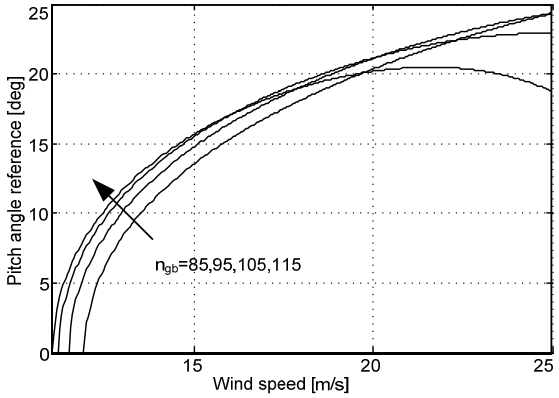


*Figure 7: Resulting pitch angle reference in full load for different gearbox ratios*

In the next step a realistic rotor inertia was found. In [4], the results from a literature research can be found. Due to limited space, it is not shown here. Finally, the rotor inertia was set to 700 kgm².
The generator inertia was computed with a CAD program and the given model of the rotor of a 2 MW DFIG. It is 85.66 kgm². These results were puplished in [4]. In the following, the dynamic simulation model will be implemented and the junction temperature variation for specific wind speeds will be simulated.

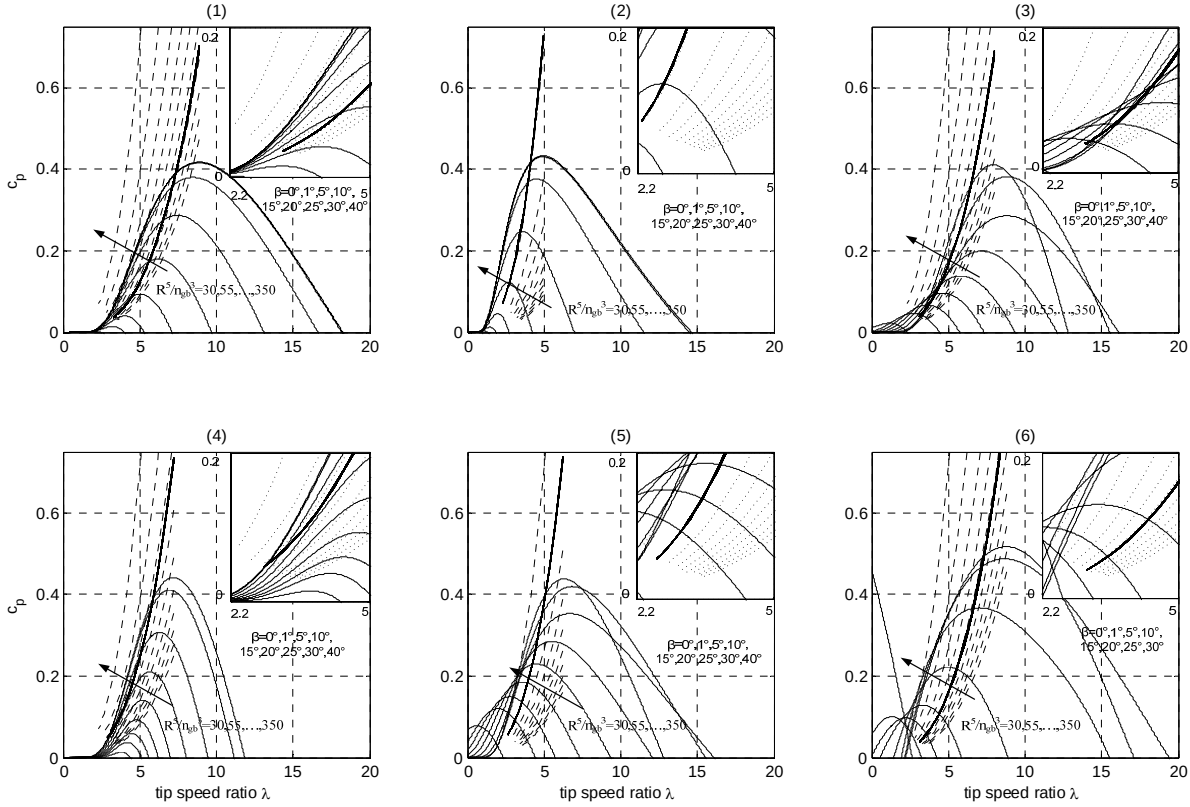


*Figure 8: Different cp characteristics from literature*

*Table 2: Cp Curve Parameters*

| | Ref. | $c_1$ | $c_2$ | $c_3$ | $c_4$ | $c_5$ | $c_6$ | $c_7$ | $c_8$ | $c_9$ | Comment | R [m] |
|---|---|---|---|---|---|---|---|---|---|---|---|---|
| 1 | [12] | 0.5 | $\frac{R\lambda_i}{\lambda}$ | 0 | 0.022 | 2 | 5.6 | $\frac{0.17R\lambda_i}{\lambda}$ | - | - | ‚MOD-2‘ turbine, 2.5 MW, 1981 | 45.72 |
| 2 | [13] | 0.5 | $\frac{Rc_f\lambda_i}{\lambda}$ | 0 | 0.022 | 2 | 2 | $\frac{0.255Rc_f\lambda_i}{\lambda}$ | - | - | $c_f$=1.9547, 250 kW, 1993 | 15 |
| 3 | [15] | 0.5 | 116 | 0.4 | 0 | 0 | 5 | 21 | 0.08 | 0.035 | - | - |
| 4 | [7] | 0.73 | 151 | 0.58 | 0.002 | 2.14 | 13.2 | 18.4 | -0.02 | -0.003 | Variable speed turbine | - |
| 5 | [16] | 0.22 | 116 | 0.4 | 0 | 0 | 5 | 12.5 | 0.08 | 0.035 | 2 MW, 2001 | 37.5 |
| 6 | [11] | - | - | - | - | - | - | - | - | - | 1.5 , 1.6, 3.6 MW, GE | - |

Results concerning the lifetime of the power semiconductors will be given. The further steps of the project will be:

- Simulation & analysis of the dynamic operation of the DFIG
- Use the existing model to extract parameter sensitivities concerning also the stochastic wind velocities
- Extend the simulation model of the PMSG to power semiconductor lifetime analysis
- Analysis of the reliability of the DC capacitors in both systems
- Building a model concerning the reliability of the whole grid connection

## 2.8.4 Motivation (IEE)

Inverter dominated components of modern offshore wind farms like doubly feed induction generators (DFIG), generators with full inverter concepts and the voltage source converter - high voltage direct current systems (VSC-HVDC) cause system perturbation with a wide frequency range. This results in a deterioration of power quality, which can lead to problems, overload and destruction of grid equipment. The offshore grid with their resources is an oscillatory system with natural frequencies. Causes the natural frequencies in the exciting frequency range of harmonic sources; this will have a negative impact on the grid operation. In this project, an approach of resonance analysis, including network reduction method is presented.

Modern wind farms feed their energy into the onshore and offshore transmission power grid via variable-speed wind turbines. These generators are equipped with inverters. Wind turbines are potential harmonic sources because of their inverter circuit feedback. The circuit feedbacks caused by power electronics have a broad frequency spectrum. The harmonics of circuit feedback cause in turn high frequency voltage and current distortions. The inverters in the self-commutated HVDC transmission systems (VSC-HVDC) for the connection of German offshore wind farms to the transmission system are also treated as harmonics generators. The natural resonant frequencies which describe the frequency characteristics of electric energy supply grids can be stimulated by harmonics. In case of equivalence between the harmonics and the natural resonant frequencies of the grid very big current or voltage distortions arises at the resonance locations. The kind of the disturbance depends on whether the harmonic-generating facility behaves either as a harmonic voltage source or harmonic current source. This results in an interference of voltage quality, which can lead to disturbances and destructions of grid equipment. In addition, negative effects on the operation of the grid are the consequence. For the description of the grid resonance behavior the calculation of grid resonances as well as the most sensitive resonance locations within the grid are required.

## 2.8.5 Approach (IEE)

To produce the most accurate results for the resonance analysis, the equipment is to be simulated for the appropriate frequency range. Within the scope of this study all the necessary equipment, such as cables, transformers, generators, DFIG and full converter generators were modeled for a frequency range from $\omega/\omega_1 = 0$ to $\omega/\omega_1 = 50$. Based on symmetrically designed grids referred to the topic of this report, equipment is modeled in the frequency range to be analyzed by symmetrical components. The grid's system of equations is needed for harmonic and resonance studies, in form of nodal admittance matrix, what can be formulated on the base of this equipment models for symmetrically designed grid systems (see figure 5).

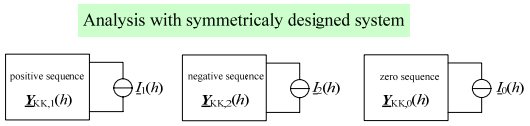


*Figure 9: Modeling of the nodal admitance matrix for harmonic and resonance analyses in symmetrically designed grids.*

**Approach for study of the grid resonance behavior**

An electrical resonance is the electromagnetic phenomenon of energy exchange between capacitive and inductive elements, which represent complementary energy storage elements. Since different grid's equipment such as e.g. transformers, overhead lines, which are modeled with inductive and capacitive elements, are connected to each other in the grid, therefore cause multiple resonant frequencies. If resonance frequencies are excited by harmonic currents or voltages, an increase of voltages and currents can appear. This leads to the disturbances of the grid equipment, and to overstrains and can cause, in the end, to the destruction of the equipment. In addition, the grid operation may be affected by resonances. Since resonances have got negative consequences on the grid behavior and the equipment, a resonance frequency analysis is necessary to be able to avoid injurious grid resonances.

Taking into consideration that resonances have a negative impact on the grid performance and the equipment, it is necessary to take an analysis of the resonant frequencies in order to avoid harmful grid resonances. The grid resonance frequency can be divided either into series resonances or parallel resonances. For the resonance studies the focus was placed on the parallel circuit, because parallel resonance frequencies can be carried out from the trend as the highest impedance into the current equation.

## 2.8.6 State of work (IEE)

The methods described above are verified by an example. The example grid topology is shown in figure 6

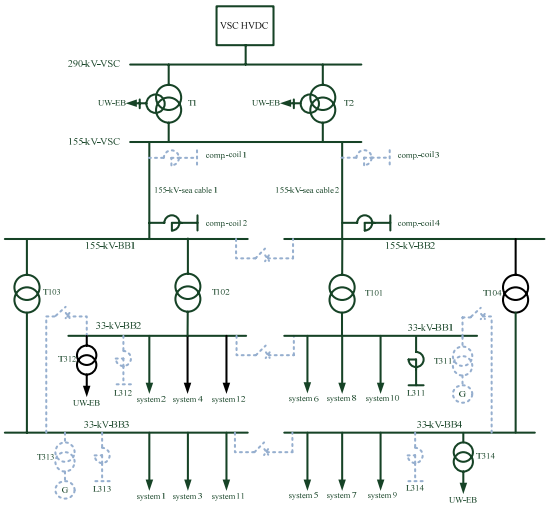


*Figure 10: Topology of an example grid*

At the four busbars compensation coils and auxiliary power are connected. At this example topology the operation of the RMA is to be clarified. There is always a possibility to determine the resonance frequency and nodes which are used to be the most sensitive for resonances. These nodes are referred to the most participation nodes. Further the grid reduction approach should be analyzed. Here the results of the entire detailed grid should be put in relation with the results of the grid equivalent. Besides, it should be shown that the grid reduction helps only for the wind park operator and leads to right results. This one would be in the position to determine the resonances clearly by frequency and by node with the grid equivalent of the transmission grid operator.

**Summary and outlook**

Based on the assumption of symmetrically designed equipment models of equipment used in the offshore grids investigated in the frequency range in symmetrical components are presented. In addition, the calculation of the parameters associated to the models is presented.

Specifically, cables, transformers, compensation coils, VSC-HVDC, DFIG and synchronous generator via full inverter with their filter circuit systems are treated. The presented models are applicable to both the grid resonance analysis and for the harmonic analysis in the low frequency range with sufficient accuracy. The formulas for the determination of the frequency dependent transformer parameters were also studied. In harmonic analyses the harmonic generators can be modeled in most cases as a frequency-dependent current source. Based on assumption in this report, problems with only the parallel resonant frequencies at which surges through harmonic current excitation and the particularly large grid impedances caused by the resonance, have been treated. Since the grid resonance frequencies with the conventional approach are not consistent and clearly to identify, a resonance analysis based on the 'Resonance Mode analysis' (RMA) in the modal components will be presented and applied. Due to the decoupling of the grid in terms of modal resonance frequencies based on the completely independent frequency, gradients of the modal impedance can be calculated exactly. The critical points of resonance that are most affected by harmonic current suggestions arise from the participation factor matrix based on determining the RMA method. In addition, the elements of the participation factor matrix show how the equipment such as compensator coil affects certain resonances in the wind farm grid. Problems with certain resonances can be avoided through a targeted change in the grid topology especially at critical points of resonance as e.g. laying a filter circuit on the adjacent grid node or a change of the switching status of the equipment. Due to the use of improved models of equipment and the effective approach for the resonance study in the modal components, the RMA is to be preferred.

In this paper the effects of mathematical grid reduction simulate both the side of the transmission system operator and the side of the wind farm operator according to the results based on selected scenarios and analyzes. On the basis of the results of the study, the grid reduction of the wind farm has strongly negative impact on the results of grid resonance study. The reason is that most of resonances caused by the wind farm. Also the most involved nodes are within the wind farm grid. Nevertheless, after the grid reduction of the wind park these are eliminated. Without the nodes involved the examination results are badly influenced. So, the grid reduction of the wind farm is not recommended for resonance studies. From the perspective of the transmission system operator, it is not sufficient to carry out the resonance studies with the grid equivalents of the wind farm for resonance analysis. Based on the results of the study the grid reduction of the transmission system operator grid has resulted comparable results as before the grid reduction. This is due to the small dimension of the offshore grid of transmission system operator. The resonances which are caused at the nodes within the grid of the wind farm operator were not recognized after the grid reduction, because such grid nodes after the reduction do not exist anymore.

The results of the grid resonance studies by the grid reduction of the grid of the transmission grid operator compared with the reduction of the wind park only easily falsifies. Thus, the reduction of the grid of transmission grid operator for the resonance analyses against the reduction of the wind farm is recommend due to small negative impact on the results of the study. From the point of view of the wind park operator, it is sufficient to carry the resonance studies with the grid equivalence impedances to reconstruct the grid of the transmission grid operator.

**References**

[1] ISET Kassel; Windenergiereport 2008 (in german).

[2] Lubosny, Z.: Wind turbine operation in electric power systems: advanced modeling and control, Springer, 2003.

[3] Bartram M.; Bloh I.; Doncker R.; Doubly-fed-machines in wind turbine systems: Is this application limiting the lifetime of IGBT frequency converters; 35th Annual IEEE Power Electronics Specialists Conference Aachen, 2004.

[4] Fuchs, F.; Mertens, A. (2012): Dynamic modeling of a 2 MW wind turbine for converter issues : part 1, Power Electronics and Motion Control (EPE PEMC 2011 ECCE Europe), Proceedings of the 2012-15th International Conference and Expositon on, Novi Sad, Serbia

[5] Arrillaga, J., Watson, N. R., Chen, S.: Power System Quality Assessment. Chichester: Wiley, 2001.

[6] Robert, A., Deflandre, T.: Guide for Assessing the Network Harmonic Impedance, CIGRE Working Group CC02, Elektra No. 167 August 1996.

[7] IEEE Std 399: IEEE Recommended Practice for Industrial and Commercial Power Systems Analysis, 1997.

[8] Papathanassiou, S. A., Papadopoulos, M. P.: Harmonic Analysis in a Power System with Wind Generation, IEEE, 2006

[9] Amornvipas, C.: Harmonic Studies and Resonance Analyses in Electrical Power Systems. Shaker Verlag, Aachen, zugl. Dissertation, Leibniz Universität Hannover, 2009.

[10] Rathke, C.: Modellierung moderner Windenergieanlagen für die Kurz-schlussstromberechnung, Diplomarbeit vom Institut für Energieversorgung und Hochspannungstechnik an der Leibniz Universität Hannover, Februar 2007.

[11] Arsudis, Dimitrios: Doppelt-gespeister Drehstromgenerator mit Spannungszwischenkreis-Umrichter im Rotorkreis für Windkraftanlagen, Dissertation an der Technischen Universität Carolo-Wilhelmina zu Braunschweig, 1989.

[12] Xu, W.: Harmonic Resonance Mode Analysis, IEEE Transactions on Power Delivery, Vol. 20, No. 2, S. 1182-1190, April 2005.

[13] Oswald, B. R.: Netzberechnung 2 – Berechnung transienter Vorgänge in Elektroenergieversorgungsnetzen. Berlin und Offenbach: VDE-VERLAG GMBH, 1996.

[14] Crastan, V.: Elektrische Energieversorgung 1. Berlin und Heidelberg: Springer-Verlag, 2000.

[15] IEC 60287-1-1: Current rating equations (100 % load factor) and calculation of losses – General, 2. Ausgabe, 2006.

# 3 Summary

**Institute of Concrete Construction**
Michael Hansen, Boso Schmidt

Finally, within this Annual report 2012 the assumptions and aims for several examinations concerning the effects and resistances of OWT are described.
Civil engineers deal with the action effects of wind and sea state on the structure and foundation. By analysis of numerical calculation and measurement data statistical approaches for action effects and stresses of the structural components are found. The soil-foundation-interaction is examined as well as dynamic load increasing. Even for the soil parameters and the force transmission from the foundation into the sea bed models based on probabilistic approaches are specified. The investigations on the overall structure are done together by several project partners. Action effects by wind and sea state including the dynamic response are treated by transfer functions for detected hot spots of the structure. Deemed essential limit states are predefined and examined by FORM and Monte-Carlo Simulation. Multiple institutes work together to solve these challenges. Step by step these tasks are done and some results are found. Within these examinations validated data were used for practical application.
For application process experimental investigations and site inspections are done. Relevant failure mechanisms as well as possible consequences are examined and documented in this report.
In WP6 condition monitoring systems for an early detection of damages in rolling element bearings are developed and tested. Therefore, novel acceleration sensors and analysis procedures are used.
Simulations of the electrical parts of OWT lead to declarations about the failure probability of single machines or grids and even for the whole offshore wind park. Therefore, electrical engineers examine eccentricities and the electromagnetic air-gap field of coils in single electrical machines with the objective to dimension diagnostic systems for winding faults, short-circuit faults or rotor eccentricities. Lifetime assessments of power semi-conductor modules strongly depend on the varying junction temperature. Suitable power characteristics were found and implemented in a model of the grid connection. For the whole wind park disturbances of the grid equipment caused by resonance frequencies are examined, too. These resonance frequencies are excited by harmonic currents or voltages and have a negative impact on the grid equipment.
All in all researchers from three faculties work together in the field of probabilistic assessment of OWT. Partially, similar methods are used to solve quite different questions. Although the application fields are different every project partner gets new impressions and ideas for his further works.

# 4 Literature

## 4.1 Publication List

### 4.1.1 Reviewed Articles

Ernst, B.; Seume J.R.:
Investigation of Site-Specific Wind Field Parameters and Their Effect on Loads of Offshore Wind Turbines.
*Energies*. 2012; 5(10):3835-3855

Lohaus, L.; Lindschulte, N.; Scholle, N.; Werner, M.:
Betontechnik für Grouted Joints – Baustoffliche und bauausführungs-technische Anforderungen.
Stahlbau 81 (2012), Heft 9

Mertens, A.; Fuchs, F.; Baruschka, L.:
Wandler im Meerespuls.
Erneuerbare Energien, 07/2012, SunMedia Verlag

### 4.1.2 Reviewed Conference Contributions

Fuchs, F.; Mertens, A.:
Dynamic modeling of a 2 MW wind turbine for converter issues: part 1.
Power Electronics and Motion Control (EPE PEMC 2011 ECCE Europe), Proceedings of the 2012-15th International Conference and Expositon on , Novi Sad, Serbia

Goretzka, J.; Rolfes, R.:
Modal and Robustness Analysis of the Support Structure of an Offshore Wind Turbine with Scattered Soil Parameters.
Proceedings of 8th PhD Seminar on Wind Energy in Europe, ETH Zürich, 2012

Lohaus, L.; Werner, M.:
Probabilistic aspects of Offshore Wind Turbines – Influence of in situ assembly of grouted joints.
Proceedings of the IALCCE Symposium, 03.10. – 06.10.2012, Vienna (A)

Wilms, M.; Schlurmann, T.:
Investigation on wave-breaking probability in deep water.
Proceedings of the 6th Chinese-German Joint Symposium on Hydraulic and Ocean Engineering, National Taiwan Ocean University, Keelung, Taiwan, September 23.-29., 2012

## 4.2 Doctoral, Diploma, Master and Bachelor Theses

Bank, S.:
Versuche zur thermografischen Aufnahme von Fließwegen verpumpter hochfester Mörtel- und Betone.
Study Thesis
IfB November 2012

Cotardo, D.:
Optimierung eines Versuchsstandes zur Untersuchung von “early-age-cycling” Effekten auf die Materialeigenschaften von Verfüllmaterial für Grouted Joints.
Study Thesis
IfB June 2012

Haberjan, L.:
Regelung eines Netzpulsstromrichters mit MATLAB/Simulink/dSpace
Study Thesis
IAL-LE November 2012

Hatzopoulos, A.; Supinski, K.:
Vergleichende Untersuchungen zwischen unterschiedlichen hochfesten Mörteln anhand eines neu entwickelten Prüfstands zur Simulation von Verfüllvorgängen an Grouted Joints.
Project Thesis
IfB November 2012

Leonardy, H.:
Entwicklung eines Excel-Tools zur Durchführung einer FMEA für Offshore-Windenergieanlagen.
Bachelor Thesis
TFD January 2012

Müller, D.:
Untersuchungen zur Entwicklung eines Messsystems zur Detektion von brechenden Wellen im Wellenbecken.
Master Thesis
IPI/FI Nov 2012

Ötting, G.:
Focused wave-breaking generated using 1st and 2nd order wave maker theory in the wave flume.
Study Thesis
FI Dez 2012

Reichert, A.; Reichert, N.:
Vergleichende Untersuchungen von Zementleim und hochfestem Mörtel für Grouted Joints.
Project Thesis
IfB July 2012

Schmitt, H.:
Untersuchung des Einflusses von Geometrieabweichungen auf die aeroelastischen Belastungen der Rotorblätter von OWEA.
Diploma Thesis
TFD March 2012

Schwanitz, F.:
Sensitivität einer Jacket-Gründungsstruktur gegenüber variierenden Wellenparametern.
Diploma Thesis
IfMa November 2012

Stein, M.:
Sensitivität einer Monopilestruktur gegenüber streuenden Wellenparametern.
Project Thesis
IfMa November 2012